TECHNICAL REPORT

AN INTEGRAL METHOD FOR THREE-DIMENSIONAL, COMPRESSIBLE, LAMINAR BOUNDARY LAYERS WITH MASS INJECTION

By: Sang-Wook Kang

CAL No. AI-2187-A-5

Prepared for:

National Aeronautics and Space Administration
Goddard Space Flight Center
Greenbelt, Maryland

Contract No. NAS 5-9978
May 1967

CORNELL AERONAUTICAL LABORATORY, INC.
OF CORNELL UNIVERSITY, BUFFALO, N. Y. 14221

CORNELL AERONAUTICAL LABORATORY, INC.
BUFFALO, NEW YORK 14221

CAL REPORT NO. AI-2187-A-5

AN INTEGRAL METHOD FOR THREE-DIMENSIONAL, COMPRESSIBLE, LAMINAR BOUNDARY LAYERS WITH MASS INJECTION

BY:
SANG-WOOK KANG

CONTRACT NO. NAS 5-9978
CAL REPORT NO. AI-2187-A-5
MAY 1967

PREPARED BY: S.W. Kang
S.W. Kang

APPROVED BY: J. Gordon Hall
J. Gordon Hall, Head
Aerodynamic Research Department

FOREWORD

The work described in this report was supported by the National Aeronautics and Space Administration, Goddard Space Flight Center, under Contract NAS 5-9978. The author gratefully acknowledges the capable assistance of Messrs. Leonard Garr and John Moselle in obtaining the computer solutions, and the useful discussions with Drs. Michael Dunn, J. Gordon Hall, and William Rae during the course of this work.

ABSTRACT

The integral method is applied to obtain a general analysis of the three-dimensional, compressible, laminar boundary layer with mass injection. The equations are expressed in terms of the streamline coordinate system and profile parameters are introduced for the streamwise velocity, the total enthalpy and the secondary-flow velocity profiles. As an illustration, the present formulation is applied to three-dimensional flow in the forebody region of a blunt body. The effects of mass injection and streamline curvature, including the effect of an inflection point in the outer inviscid streamline, are analyzed. The nonsimilar nature of the three-dimensional boundary-layer flow is observed.

TABLE OF CONTENTS

LIST OF ILLUSTRATIONS

LIST OF SYMBOLS

A	Streamwise wall-shear parameter, $\left(\frac{\partial U}{\partial \eta}\right)_b$
a	Constant, $\frac{3\sqrt{\pi}}{2}$
B	Heat-transfer parameter, $\left(\frac{\partial \theta}{\partial \eta}\right)_b$
C	Secondary- flow wall-shear parameter, $\left(\frac{\partial V}{\partial \eta}\right)_b = \frac{a^3 G - Q}{a^2 + W}$
C'	Coefficient for viscosity; Eq. (17)
D_1	Dimensionless streamline curvature, $K_1 \ell$, Eq. (19)
E_2	Dimensionless metric coefficient, e_2 / e_{2_r}
e_1, e_2	Metric coefficients in curvilinear coordinate system, Eq. (1)
F_i	Functions defined in Sec. II-C
f	Dimensionless (Howarth-Dorodnitzyn) stream function in Sec. II-D
G, F	Profile parameters for secondary-flow velocity, Eq. (37)
g	Profile function, Eq. (38)
H	Total enthalpy, $h + \frac{u^2 + w^2}{2}$
h	Static enthalpy
H_i	Total enthalpy-defect thickness, Eq. (15)
k	Profile function, Eq. (38)
K_1, K_2	Geodesic curvature of streamlines, Eq. (7)
ℓ	Body nose radius
M_i	Dimensionless displacement thickness, Eq. (44), $\frac{\delta_i}{\Delta}$
M_{ij}	Dimensionless momentum-defect thickness, Eq. (44), $\frac{\delta_{ij}}{\Delta}$
m_i	Profile functions, Eqs. (31) and (36)
N	Mass injection ratio, $\frac{\rho_b w_b}{\rho_0 u_0}$

LIST OF SYMBOLS (Cont.)

P	Dimensionless pressure-gradient parameter, Eq. (25)
P_i	Constants defined in Appendix
Pr	Prandtl number
p	Pressure
Q	Dimensionless streamline-curvature parameter, Eq. (25)
Q_1	$\frac{Q}{a^2+W}$, Eq. (43)
r	Distance from the body surface to the axis of symmetry
Re	Reynolds number, $\frac{\rho_0 u_0 \ell}{\mu_0}$
S	Sutherland constant, Eq. (18)
s	Line element, Eq. (1)
T_i	Dimensionless total enthalpy-defect thickness, Eq. (44) $\frac{H_i}{\Delta}$
U	Dimensionless streamwise velocity, $\frac{u}{u_e}$
V	Dimensionless secondary-flow (transverse) velocity, $\frac{v}{u_e}$
W	Dimensionless mass-injection parameter, Eq. (19)
W_p	$Pr_b W$
W_1	$\frac{aW}{a^2+W}$, Eq. (43)
u, v, w	Velocities in curvilinear coordinate directions (Fig. 1)
x, y, z	Curvilinear coordinates (Fig. 1)
X	Dimensionless distance along streamline, $\frac{e_1 dx}{\ell}$
Z	Transformed coordinate normal to the body surface, Eq. (16)
α	Defined in Eq. (67), $\tan^{-1}\left(\frac{C}{A}\right)$
β	Defined in Eq. (61)
β^*	Pressure-gradient parameter, $\frac{2\xi}{u_e}\frac{H_e}{h_e}\frac{du_e}{d\xi}$

LIST OF SYMBOLS (Cont.)

γ	Specific-heat ratio
Δ	Transformed boundary-layer thickness, Eq. (16)
δ	Physical boundary layer thickness
δ_i	Displacement thickness, Eq. (15)
δ_{ij}	"Moment-defect" thickness, Eq. (15)
η	$\frac{z}{\Delta}$
θ	Total enthalpy ratio, $\frac{H}{H_e}$
μ	Viscosity
ν	Kinematic viscosity
ξ, η^*	Howarth-Dorodnitzyn transformation coordinates, Eq. (68)
ρ	Mass density
τ_i	Wall-shear stress, Eq. (71)
ϕ	Coordinate normal to streamlines
ψ	Stream function
Ω	Dimensionless boundary-layer thickness, $\frac{\Delta}{\ell}\sqrt{R_e}$

Subscripts

b	Surface condition
e	Local value at the outer edge of the boundary layer
r	Reference condition
o	Condition behind a normal shock
∞	Free-stream condition

NOTE: Bar over symbol signifies dimensionless variables.

I. INTRODUCTION

Analysis of three-dimensional boundary-layer flows has been the subject of increasing interest because of its application to lifting vehicles entering the atmosphere with hypersonic speeds. Review articles are available, for example, by Cooke and Hall[1], Mager[2], Moore[3], and Rosenhead[4].

Many analyses on three-dimensional boundary-layer flows have been performed for special geometries, where simplifications in the governing equations are possible, such as yawed infinite cylinders[5-7] and flat plates[8-11]. Numerous analyses are also available for other special cases, as, for example, a blunt-nosed cold body[12], and flows where the secondary-flow (transverse) velocity component is assumed to be small compared with the streamwise velocity[13-22]. Flows in the stagnation region have also been analyzed[23-26].

The complexity of the equations for three-dimensional, compressible boundary-layer flows makes it difficult to obtain general, analytic solutions. The present analysis treats the full three-dimentional boundary-layer equations, including mass injection at the body surface, by employing the integral method. Although the method is approximate, involving assumption of the profile forms for velocity and temperature, it nevertheless yields satisfactory nonsimilar solutions for the boundary-layer flow. Assumptions concerning similarity or local similarity of the flow characteristics or the magnitude of the secondary-flow velocity component are not introduced in the present analysis. For simplicity, however, the ideal-gas equation of state is assumed.

The basic integral equations are derived in Section II-A. In Section II-B, the choice of profiles is discussed and in Section II-C, the final formulation of the integral equations is made, along with application to several special cases and comparison with previous results. In Section II-D, sample solutions are obtained for flows on an Apollo-type blunt body and a discussion of the results is presented. The effects of mass injection on three-dimensional boundary layers are discussed in detail.

II. ANALYSIS

II-A Basic Equations

The curvilinear coordinate system used in the present analysis is shown in Fig. 1. The x-coordinate coincides with the local external inviscid streamline projected on the plane tangent to the body surface. The y-coordinate is also in the tangent plane and is normal to x, and z-coordinate is in the direction normal to the tangent plane. In the special case where the inviscid flow is irrotational, the y-constant lines then become the potential-flow lines. The corresponding velocities are u, v and w. The line element is given by

$$(ds)^2 = (e_1 dx)^2 + (e_2 dy)^2 + (dz)^2 \tag{1}$$

For the case of a nonreacting gas, the equations for a compressible, three-dimensional boundary layer are[1, 2, 27]

Continuity

$$\frac{1}{e_1 e_2}\frac{\partial}{\partial x}(\rho u e_2) + \frac{1}{e_1 e_2}\frac{\partial}{\partial y}(\rho v e_1) + \frac{\partial}{\partial z}(\rho w) = 0 \tag{2}$$

x-momentum

$$\frac{\rho u}{e_1}\frac{\partial u}{\partial x} + \frac{\rho v}{e_2}\frac{\partial u}{\partial y} + \rho w \frac{\partial u}{\partial z} + K_1 \rho u v - K_2 \rho v^2 = -\frac{1}{e_1}\frac{\partial p}{\partial x} + \frac{\partial}{\partial z}\left(\mu \frac{\partial u}{\partial z}\right) \tag{3}$$

y-momentum

$$\frac{\rho u}{e_1}\frac{\partial v}{\partial x} + \frac{\rho v}{e_2}\frac{\partial v}{\partial y} + \rho w \frac{\partial v}{\partial z} + K_2 \rho u v - K_1 \rho u^2 = -\frac{1}{e_2}\frac{\partial p}{\partial y} + \frac{\partial}{\partial z}\left(\mu \frac{\partial v}{\partial z}\right) \tag{4}$$

z-momentum

$$\frac{\partial p}{\partial z} = 0 \tag{5}$$

Energy

$$\frac{\rho u}{e_1}\frac{\partial H}{\partial x} + \frac{\rho v}{e_2}\frac{\partial H}{\partial y} + \rho w \frac{\partial H}{\partial z} = \frac{\partial}{\partial z}\left(\frac{\mu}{Pr}\frac{\partial H}{\partial z}\right) - \frac{\partial}{\partial z}\left[\frac{\mu(1-Pr)}{2Pr}\frac{\partial}{\partial z}(u^2+v^2)\right] \tag{6}$$

where

$$H = h + \frac{u^2 + v^2}{2}$$

$$K_1 = \frac{1}{e_1 e_2} \frac{\partial e_1}{\partial y}, \qquad K_2 = \frac{1}{e_1 e_2} \frac{\partial e_2}{\partial x} \tag{7}$$

The boundary conditions are

$$u(x, y, 0) = v(x, y, 0) = 0$$

$$w(x, y, 0) = w_b(x, y)$$

$$H(x, y, 0) = H_b = h_b(x, y)$$

$$u(x, y, \infty) = u_e(x, y)$$

$$v(x, y, \infty) = 0$$

$$H(x, y, \infty) = H_e = h_e + \frac{u_e^2}{2}$$

Applying Eqs. (3) and (4) at the outer edge of the boundary layer, and taking Eq. (5) into account, one obtains

$$\frac{\rho_e u_e}{e_1} \frac{\partial u_e}{\partial x} = -\frac{1}{e_1} \frac{\partial p}{\partial x}$$

$$K_1 \rho_e u_e^2 = \frac{1}{e_2} \frac{\partial p}{\partial y} \tag{9}$$

Substitution of Eq. (9) in Eqs. (3) and (4) yields

$$\frac{\rho u}{e_1} \frac{\partial u}{\partial x} + \frac{\rho v}{e_2} \frac{\partial u}{\partial y} + \rho w \frac{\partial u}{\partial z} + K_1 \rho u v - K_2 \rho v^2 = \frac{\rho_e u_e}{e_1} \frac{\partial u_e}{\partial x} + \frac{\partial}{\partial z}\left(\mu \frac{\partial u}{\partial z}\right) \tag{10}$$

$$\frac{\rho u}{e_1} \frac{\partial v}{\partial x} + \frac{\rho v}{e_2} \frac{\partial v}{\partial y} + \rho w \frac{\partial v}{\partial z} + K_2 \rho u v = K_1 \rho u_e^2 \left[\left(\frac{u}{u_e}\right)^2 - \frac{\rho_e}{\rho}\right] + \frac{\partial}{\partial z}\left(\mu \frac{\partial v}{\partial z}\right) \tag{11}$$

Equations (6), (10), and (11) are now integrated from $z = 0$ to $z = \delta$ and, combined with the continuity Eq. (2), become

$$\frac{1}{\rho_e u_e^2 e_1}\frac{\partial}{\partial x}\left(\rho_e u_e^2 \theta_{11}\right) + \frac{1}{e_2}\frac{\partial \theta_{12}}{\partial y} + \frac{\delta_1}{u_e e_1}\frac{\partial u_e}{\partial x} + K_2\left(\theta_{11} + \theta_{22}\right)$$

$$+ \theta_{12}\left(K_1 + \frac{2}{u_e e_2}\frac{\partial u_e}{\partial y} + \frac{1}{\rho_e e_2}\frac{\partial \rho_e}{\partial y}\right) - \delta_2\left(K_1 + \frac{1}{u_e e_2}\frac{\partial u_e}{\partial y}\right)$$

$$= \frac{\mu_b}{\rho_e u_e^2}\left(\frac{\partial u}{\partial z}\right)_b + \frac{\rho_b w_b}{\rho_e u_e} \tag{12}$$

$$\frac{1}{\rho_e u_e^2 e_1}\frac{\partial}{\partial x}\left(\rho_e u_e^2 \theta_{21}\right) + \frac{1}{e_2}\frac{\partial \theta_{22}}{\partial y} + 2K_2\theta_{21} + K_1\left(\theta_{11} + \delta_1\right)$$

$$+ \theta_{22}\left(K_1 + \frac{2}{u_e e_2}\frac{\partial u_e}{\partial y} + \frac{1}{\rho_e e_2}\frac{\partial \rho_e}{\partial y}\right) = -\frac{\mu_b\left(\frac{\partial v}{\partial z}\right)_b}{\rho_e u_e^2} \tag{13}$$

and

$$\frac{\partial H_1}{e_1 \partial x} + \frac{\partial H_2}{e_2 \partial y} + H_1\left(K_2 + \frac{1}{\rho_e e_1}\frac{\partial \rho_e}{\partial x} + \frac{1}{u_e e_1}\frac{\partial u_e}{\partial x}\right)$$

$$+ H_2\left(K_1 + \frac{1}{u_e e_2}\frac{\partial u_e}{\partial y} + \frac{1}{\rho_e e_2}\frac{\partial \rho_e}{\partial y}\right) \tag{14}$$

$$= \frac{\mu_b}{\rho_e u_e Pr_b}\left(\frac{\partial \theta}{\partial z}\right)_b + \frac{\rho_b w_b}{\rho_e u_e}\theta_b$$

where

$$\delta_1 = \int_0^\delta \left(\frac{\rho_e}{\rho} - \frac{u}{u_e}\right)\frac{\rho}{\rho_e}\,dy \qquad \delta_2 = \int_0^\delta \frac{w}{u_e}\frac{\rho}{\rho_e}\,dy$$

$$\delta_{11} = \int_0^\delta \left(1 - \frac{u}{u_e}\right)\frac{u}{u_e}\frac{\rho}{\rho_e}\,dy \qquad \delta_{12} = \int_0^\delta \frac{w}{u_e}\left(1 - \frac{u}{u_e}\right)\frac{\rho}{\rho_e}\,dy$$

$$\delta_{21} = \int_0^\delta \frac{u\,w}{u_e^2}\frac{\rho}{\rho_e}\,dy \qquad \delta_{22} = \int_0^\delta \left(\frac{w}{u_e}\right)^2\frac{\rho}{\rho_e}\,dy$$

$$H_1 = \int_0^\delta (1-\theta)\frac{u}{u_e}\frac{\rho}{\rho_e}\,dy \qquad H_2 = \int_0^\delta (1-\theta)\frac{w}{u_e}\frac{\rho}{\rho_e}\,dy \qquad (15)$$

It should be noted here that the momentum boundary-layer thickness (δ) is taken to be the same for both the streamwise and the secondary flows. This seems to be a reasonable step to take, based on comparisons with the exact solutions obtained by Hansen, et al[28-32], and other solutions obtained, for example, by Cooke[17], Beckwith[19], and Kang, Rae, and Dunn[16]. Further, the thermal boundary-layer thickness is assumed to be the same as the momentum boundary-layer thickness which is consistent with the assumption of others such as Poots[33] and Libby and Pallone[34]. The term $\rho_b w_b$ signifies the mass-injection flux at the body surface. When this term is equal to zero, ie., the solid-wall case, Eqs. (12), (13), and (14) reduce to the equations obtained in Refs. 1 and 2.

The y-coordinate is now transformed by introducing the Dorodnitzyn variable

$$Z = \int_0^y \frac{\rho}{\rho_e}\,dy \qquad (16)$$

from which follows the boundary-layer thickness in the transformed plane

$$\Delta = \int_0^\delta \frac{\rho}{\rho_e}\,dy$$

In addition, the viscosity term is assumed to vary with temperature[35], as follows

$$\frac{\mu}{\mu_o} = C' \frac{T}{T_o} \tag{17}$$

where the subscript o denotes reference conditions and the coefficient is taken such that the Sutherland viscosity-temperature relation is exactly satisfied at the wall temperature T_b. Thus,

$$C' = \sqrt{\frac{T_b}{T_o}} \left(\frac{T_o + S}{T_b + S} \right) \tag{18}$$

where S is the Sutherland constant.

In order to make the formulation as general as possible, the equations are nondimensionalized with respect to a reference condition. A suitable reference point is, for example, the point immediately behind the shock on the stagnation streamline. Thus, we introduce

$$\Omega = \frac{\Delta}{\ell} \sqrt{Re} \qquad Re = \frac{\rho_o u_o \ell}{\mu_o}$$

$$U = \frac{u}{u_e} \qquad \bar{u}_e = \frac{u_e}{u_o}$$

$$V = \frac{v}{u_e} \qquad D_1 = K_1 \ell$$

$$W = N \frac{\bar{\rho}_e \sqrt{Re}}{\bar{\rho}_b \bar{\mu}_b} \Omega \qquad N = \frac{\rho_b w_b}{\rho_o u_o} \tag{19}$$

and

$$M_{ij} = \frac{\delta_{ij}}{\Delta} \qquad T_i = \frac{H_i}{\Delta}$$

$$M_i = \frac{\delta_i}{\Delta} \qquad \eta = \frac{z}{\Delta} \tag{20}$$

where terms with bars signify normalization with respect to the reference condition, e.g., $\bar{\rho}_e = \frac{\rho_e}{\rho_o}$ etc. In addition, the term E_2 will be introduced as $E_2 = \frac{e_2}{e_{2r}}$ where e_{2r} is the metric coefficient at some convenient point in the flow and is a constant. Then Eqs. (12), (13), and (14) become, after some rearrangements,

$$\frac{\partial \Omega^2}{e_1 \partial(x/\ell)} + \Omega^2 \frac{2}{e_1} \frac{\partial}{\partial(x/\ell)} \left[\ln \bar{\rho}_e \bar{u}_e^{2+\frac{M_1}{M_{11}}} M_{11} E_2^{1+\frac{M_{22}}{M_{11}}} \right]$$

$$= \frac{2}{M_{11}} \left(\frac{\rho_b}{\rho_e} \right) \frac{\bar{\mu}_b}{\bar{\rho}_e \bar{u}_e} \left[\left(\frac{\partial U}{\partial \eta} \right)_b + W \right] + \frac{2\Omega^2}{e_2} \frac{M_2}{M_{11}} \frac{\partial}{\partial(y/\ell)} (\ln e_1 u_e)$$

$$- \frac{2\Omega^2}{e_2} \frac{M_{12}}{M_{11}} \frac{\partial}{\partial(y/\ell)} \left[\ln e_1 u_e^2 \bar{\rho}_e \right] - \frac{2\Omega}{M_{11} e_2} \frac{\partial \left[(\Omega M_{12} \sqrt{Re})/\ell \right]}{\partial(y/\ell)} \quad , \tag{21}$$

$$\frac{\partial (M_{21} \Omega)}{e_1 \partial(x/\ell)} + \frac{M_{21} \Omega}{e_1} \frac{\partial}{\partial(x/\ell)} \left[\ln \bar{\rho}_e \bar{u}_e^2 E_2^2 \right]$$

$$= -D_1 \Omega (M_{11} + M_1) - \left(\frac{\rho_b}{\rho_e} \right) \frac{\bar{\mu}_b}{\bar{\rho}_e \bar{u}_e \Omega} \left(\frac{\partial V}{\partial \eta} \right)_b$$

$$- \frac{M_{22} \Omega}{e_2} \frac{\partial}{\partial(y/\ell)} \left[\ln e_1 u_e^2 \bar{\rho}_e \right] - \frac{1}{e_2} \frac{\partial \left[(\Omega M_{22} \sqrt{Re})/\ell \right]}{\partial(y/\ell)} \quad , \tag{22}$$

and

$$\frac{\partial(T_1\Omega)}{e_1\,\partial(x/\ell)} + \frac{T_1\Omega}{e_1}\,\frac{\partial}{\partial(x/\ell)}\left[\ln \bar{\rho}_e\,\bar{u}_e\,E_2\right]$$

$$= \left(\frac{\rho_b}{\rho_e}\right)\frac{\bar{\mu}_b}{\bar{\rho}_e\,\bar{u}_e\,\Omega}\left[\frac{1}{Pr_b}\left(\frac{\partial\theta}{\partial\eta}\right)_b + W\theta_b\right]$$

$$- \frac{T_2\Omega}{e_2}\,\frac{\partial}{\partial(y/\ell)}\left[\ln e_1\,u_e\,\bar{\rho}_e\right] - \frac{\partial(T_2\Omega)}{e_2\,\partial(y/\ell)} \qquad (23)$$

It may be noted here that the integral equations, Eqs. (21), (22), and (23), have the following properties.

i. They can accommodate mass injections at the body surface. The term W contains the mass injection flux and appears in Eqs. (21) and (23).

ii. They can be used for both laminar and turbulent boundary-layer flows. In the case of a turbulent flow, some suitable correlations may be used for the reference temperature, $\left(\frac{\partial u}{\partial\eta}\right)_b$, $\left(\frac{\partial v}{\partial\eta}\right)_b$ and $\left(\frac{\partial\theta}{\partial\eta}\right)_b$ to obtain the solutions. (See, for example, Refs. 36-41).

The integral equations yield integrated effects of the flow characteristics from an upstream location to a point of interest in the flow field. In obtaining meaningful solutions, however, it is also important to account for local effects such as mass injection at the body surface and local pressure gradients tangent and transverse to the streamline. For this latter purpose, the so-called "compatibility conditions" at the wall are introduced, by specializing the differential equations (6), (10), and (11) to the body surface. Thus, we obtain, in dimensionless forms,

$$W\left(\frac{\partial u}{\partial\eta}\right)_b = P + \left(\frac{\partial^2 u}{\partial\eta^2}\right)_b \qquad (24a)$$

$$W\left(\frac{\partial v}{\partial\eta}\right)_b = -Q + \left(\frac{\partial^2 v}{\partial\eta^2}\right)_b \qquad (24b)$$

$$W\left(\frac{\partial\theta}{\partial\eta}\right)_b = \frac{1}{Pr_b}\left(\frac{\partial^2\theta}{\partial\eta^2}\right)_b - \left(\frac{u_e^2}{H_e}\right)\left(\frac{1-Pr}{Pr}\right)_b\left[\left(\frac{\partial U}{\partial\eta}\right)_b^2 + \left(\frac{\partial V}{\partial\eta}\right)_b^2\right] \tag{24c}$$

where

$$P = \left(\frac{\rho_e}{\rho_b}\right)^2 \frac{\bar{\rho}_e}{\bar{\mu}_b} \frac{\Omega^2}{e_1} \frac{\partial \bar{u}_e}{\partial(x/\ell)}$$

$$Q = D_1 \Omega^2 \frac{\bar{\rho}_e \bar{u}_e}{\bar{\mu}_b}\left(\frac{\rho_e}{\rho_b}\right)^2 \tag{25}$$

For the region near the stagnation point in hypersonic flows, u_e^2/H_e is much smaller than unity and, thus, the last term in Eq. (24c) may be neglected without loss in accuracy, although the Prandtl number may not be unity. In the case where the Prandtl number is unity, of course, the term is identically zero. In obtaining the examples included in this report, the term containing u_e^2/H_e is neglected in order to save computation time. However, if necessary, this term may be left in the equation and the formulation will follow the same procedure. Thus, we have

$$W\left(\frac{\partial\theta}{\partial\eta}\right)_b \cong \frac{1}{Pr_b}\left(\frac{\partial^2\theta}{\partial\eta^2}\right)_b \tag{26}$$

We now have derived six equations, viz., Eqs. (21), (22), (23), (24a), (24b), and (26). Thus, six unknown parameters describing the flow characteristics may be introduced and, theoretically, the problem is determinate. It is the manner of choosing these parameters that forebodes success or failure in obtaining meaningful solutions for the flow-field characteristics by application of the integral method. In the following section, several techniques that have been applied in the past will be reviewed and the choice of profiles for the present analysis will be discussed.

II-B Choice of Profiles

Application of the integral method to the boundary-layer flow involves assuming forms of the velocity and total enthalpy profiles in terms of parameters which characterize the fluid motion. The commonly used techniques in two-dimensional and axisymmetric cases are due to Pohlhausen[13, 22, 34, 42-46], Thwaites[47-49], Timman[50], Dorodnitzyn[51-53], and Head[54-55]. In the Pohlhausen technique, the profiles are assumed in polynomial forms, and parameters are expressed by satisfying the boundary conditions at the body and at the outer edge of the boundary layer. These parameters are then obtained by solving the integral equations. This approach has been used most extensively because of its great simplicity in application. In Timman's approach, the profiles are expressed in terms of the error function and all derivatives of these profiles asymptotically approach zero at the outer edge of the boundary layer and, thus, the boundary conditions there are identically satisfied. The Dorodnitzyn scheme involves dividing the boundary layer into strips, and in each strip the polynomial distribution is assumed. Thus, this approach is an extended version of the Pohlhausen method. The method due to Head introduces doubly-infinite family of profiles based on exact solutions and, by satisfying the compatibility condition and the integral equation, solutions are obtained. Lastly, the Thwaite's approach is based on determining the variations of the assumed parameters from similar solutions, thereby obtaining a simple quadrature for the solution.

With some simplifying assumptions, such as incompressible flow, no mass injection, or small secondary-flow velocity, these approaches have been extended to the three-dimensional cases (see, for example, Refs. 1, 13, 15, 17, 18, 20, 22, 40, 44, 56-61). It has been found from these analyses, especially from Refs. 1 and 58, that when the flow is expressed in the streamline coordinate system, the streamwise flow behaves like a two-dimensional boundary layer, even when the other component, i.e., the secondary (or transverse) flow, is appreciable. This is an important result, since it suggests the application of the technique used in the two-dimensional case to the streamwise flow in three-dimensional flow with reasonable confidence. It

also suggests that interpretations of the results from the two-dimensional flow analyses may be applicable in a qualitative way to the streamwise flow in the three-dimensional case. In particular, the relative merits of these various methods may be inferred for the three-dimensional case from their relative values and accuracies when applied in the two-dimensional case. By comparison of these methods, it was found that their relative accuracies varied significantly for the adverse pressure gradient cases. However, when the pressure gradient was "favorable", that is, when the flow was accelerating, all of these methods showed remarkably similar results. Of course, the more elaborate (and thus more laborious) yielded slightly more accurate results. On the whole, however, one of the simpler methods, i.e., the Pohlhausen polynomial method, gave very reasonable results in two-dimensional flows[34, 35, 45, 49], even in the case of mass injection at the body surface[43, 46, 62]. Thus, because of its overall advantages, such as simplicity in application, resultant saving in labor (computation time), and reasonable results, it was decided to apply the Pohlhausen polynomial method to the streamwise-flow velocity profile and to the total-enthalpy profile. For the secondary-flow velocity profile, however, it was anticipated that there would be, in general, an inflection point in the streamline which brings about reversal of the flow direction of the secondary-flow velocity component. In order to accommodate this, and in order to give more accurate profile distribution for the secondary-flow velocity, Timman's[63-64] approach (subsequently refined by Zaat[15] and Cooke[18]) is extended here for the compressible case with or without mass injection. Comparison is also made with the analysis of Ref. 16 for the special case of small secondary flow. In the following, the profiles will be determined in terms of the parameters which describe the boundary-layer flow characteristics.

The Streamwise Velocity Profile

We introduce the fourth-degree polynomial form

$$U = \frac{u}{u_e} = \sum_{m=0}^{4} a_m \eta^m \tag{27}$$

The boundary conditions are

$$\eta = 0 ; \qquad U = 0$$

$$\eta = 1 ; \qquad U = 1$$

$$\frac{\partial U}{\partial \eta} = 0$$

$$\frac{\partial^2 U}{\partial \eta^2} = 0 \tag{28}$$

In addition, we have the compatibility condition at the wall, i.e., Eq. (24a). Substitution of Eq. (27) in Eqs. (24a) and (28) gives

$$a_0 = 0$$

$$a_1 = \frac{12 + P}{6 + W} = A$$

$$a_2 = \frac{W a_1 - P}{2}$$

$$a_3 = 4 + P - a_1 (3 + W)$$

$$a_4 = -3 - \frac{P}{2} + a_1 \left(2 + \frac{W}{2}\right) \tag{29}$$

Therefore, we have

$$U = m_1(\eta) + A\, m_2(\eta) \tag{30}$$

where

$$m_1(\eta) = \eta^2 \left(6 - 8\eta + 3\eta^2\right)$$

$$m_2(\eta) = \eta \left(1 - \eta\right)^3 \tag{31}$$

The functions m_1 and m_2 are plotted in Fig. 2 and $U(\eta)$ in Fig. 3. Thus, the streamwise velocity is expressed as a function of only one parameter, A. The physical significance of A is that it expresses the magnitude of the velocity gradient at the body surface and, therefore, is a measure of the streamwise shear stress. It is interesting to note here that when there is no mass injection at the wall, $W = 0$, then A is dependent only on P, the pressure-gradient parameter. On the other hand, if the mass injection is very great, the other limiting case is obtained, i.e., $A \longrightarrow 0$, as $W \longrightarrow \infty$. In other words, as mass injection increases, the streamwise skin friction decreases and in the limit approaches zero, a physically reasonable result. Another interesting result is that when there is no streamwise pressure gradient, i.e., $P \equiv 0$, $A = \frac{12}{6 + W}$. If in addition, $W = 0$, that is, solid wall, we have the result, $A = 2$, and the velocity profile for this case agrees with the Blasius profile. It may also be seen that regardless of the value of W, $A = 0$ for $P = -12$, signifying the separation of the flow due to adverse pressure gradient. Later in Section II-D, numerical comparison of the value of A will be made with other results for the more general case of finite pressure gradient and mass injection.

We have thus expressed the streamwise velocity profile in terms of one parameter, which combines the pressure-gradient characteristic and the mass-injection characteristics in the flow. It should be noted here once again that, based on previous analyses, the above one-parameter expression is expected to yield reasonable results. Caution is advised in the adverse pressure-gradient case, although Poots[33] seems to have obtained good results from the application of the fourth-order polynomials for the profiles.

The Total-Enthalpy Profile

Here, we introduce the fifth-degree polynomial form such that

$$\theta = \frac{H}{H_e} = \sum_{m=0}^{5} b_m \eta^m \tag{32}$$

The reason for taking this particular form is discussed later.

The boundary conditions are

$$\eta = 0 \; ; \qquad \theta = \theta_b$$

$$\eta = 1 \; ; \qquad \theta = 1$$

$$\frac{\partial \theta}{\partial \eta} = 0$$

$$\frac{\partial^2 \theta}{\partial \eta^2} = 0 \tag{33}$$

The compatibility condition for the total enthalpy is given in Eq. (26). We thus obtain

$$\begin{aligned} b_0 &= \theta_b \\ b_1 &= B \\ b_2 &= \frac{W_p}{2} b_1 \\ b_3 &= 10(1-b_0) - \left(6 + \tfrac{3}{2} W_p\right) b_1 \\ b_4 &= -15(1-b_0) + \left(8 + \tfrac{3}{2} W_p\right) b_1 \\ b_5 &= 6(1-b_0) - \left(3 + \frac{W_p}{2}\right) b_1 \end{aligned} \tag{34}$$

where $W_p = Pr_b W$

and Eq. (32) becomes

$$\frac{\theta - \theta_b}{1 - \theta_b} = m_5(\eta) + \frac{B}{1-\theta_b}\left[m_4(\eta) + W_p\, m_3(\eta)\right] \tag{35}$$

where

$$m_3(\eta) = \frac{\eta^2}{2}(1-\eta)^3$$

$$m_4(\eta) = \eta(1 - 6\eta^2 + 8\eta^3 - 3\eta^4)$$

$$m_5(\eta) = \eta^3(10 - 15\eta + 6\eta^2) \tag{36}$$

The distributions of these functions along η are shown in Figs. 4-6. In contrast to the streamwise flow case, where the fourth-degree polynomial form is used, the total-enthalpy profile here is expressed in fifth-degree polynomial form. The reason is as follows: if only fourth-degree form were used, all b_m's can be determined in terms of W, P, θ_b and A and, thus, the problem is reduced to obtaining the solutions to the streamwise-momentum integral equation. Once the solutions are obtained for A, W, P from the equation, then, it is a simple matter to construct the total-enthalpy characteristics, and the energy equation, i.e., the total-enthalpy integral equation, is ignored. This procedure has been used by Cohen and Reshotko[48] using Thwaite's approach and the results show, in some cases, poor accuracy in the energy field while yielding the velocity field accurately. Others (such as Tani[65] and Poots[33]) use the energy equation and the fourth-degree form. They then drop the compatibility condition, but in its place use the "kinetic-energy" integral equation and obtain good results. Physically, the energy equation and the compatibility condition serve two functions; the energy integral equation describes the integrated effects of the energy of the flow from upstream to the point of interest along the streamline, while the compatibility condition describes the local flow effects. It is thus recognized that meaningful results may be obtained by considering both equations. This procedure has, in fact, been followed in two-dimensional cases[34, 49]. In the present analysis, therefore, both the energy integral equation and the compatibility conditions are retained and considered by assuming a fifth-order polynomial form for the total-enthalpy profile. It should be noted, however, that the results for the energy field can be interpreted only in conjunction with

the streamwise momentum results, as well as the secondary-flow momentum results.

The Secondary-Flow Velocity Profile

In the present analysis, we assume a modified form of Timman's profile, such that

$$V = \frac{v}{u_e} = G\, k(\eta) - F\, g(\eta) \tag{37}$$

where

$$k(\eta) = a\,\eta\, e^{-a^2\eta^2}$$

$$g(\eta) = \frac{1}{2}\left[\operatorname{erfc}(a\eta) + (\eta - 1)\, e^{-a^2\eta^2}\right]$$

$$a = 3\pi/2 \tag{38}$$

Figure 7 shows the distributions of k and g along η. The profiles of $V(\eta)$ for various values of G and F are plotted in Figs. 8-10. The terms G and F are two free parameters which will be determined from the integral equations and the compatibility conditions. In fact, the compatibility condition can be used at this juncture to eliminate one parameter, thus leaving the integral equation to solve for the remaining parameter along the streamline.

Substitution of Eq. (37) in Eq. (24b) yields

$$W(aG + F) = -Q - a^2 F \tag{39}$$

Thus,

$$F = -\frac{Q + aWG}{a^2 + W} \tag{40}$$

Since the wall-shear for the secondary flow is $\left(\frac{\partial V}{\partial \eta}\right)_b = aG + F$, use of Eq. (40) gives

$$C = \left(\frac{\partial V}{\partial \eta}\right)_b = \frac{a^3 G - Q}{a^2 + W} \tag{41}$$

Thus, the profile becomes, from Eq. (40),

$$V(\eta) = G\, k(\eta) + (W_1 G + Q_1)\, g(\eta) \tag{42}$$

where

$$W_1 = \frac{aW}{a^2 + W}$$

$$Q_1 = \frac{Q}{a^2 + W} \tag{43}$$

It should be noted that presence of an inflection point along the streamline may cause the secondary-flow velocity profile to be S-shaped (or "cross-over" profile) near the inflection point. Thus, in order to obtain realistic velocity distributions, it is necessary for the profile to exhibit the S-shaped form, as well as the C-shaped form. This requirement is satisfied by the profile form assumed in Eq. (37) or Eq. (42), and the problem now is to determine from the integral equations the values of these parameters, i.e., G and F, along the streamline.

With the chosen profile forms, it is now possible to calculate various characteristic "thicknesses" from these profiles in terms of parameters A, B, G, etc.

From Eqs. (15) and (20), we have

$$M_{11} = \int_c^1 U(1-U)\,d\eta = P_1 + P_2 A - P_3 A^2$$

$$M_{21} = \int_0^1 U V\,d\eta = G(P_4 + A P_5 + W_1 P_6 + A W_1 P_7) + Q_1 (P_6 + A P_7)$$

$$M_2 = \int_0^1 V\,d\eta = G(P_8 + W_1 P_9) + Q_1 P_9$$

$$M_{12} = \int_0^1 V(1-U)\,d\eta = M_2 - M_{21}$$

$$M_{22} = \int_0^1 V^2\,d\eta = G^2(P_{10} + 2W_1 P_{11} + W_1^2 P_{12}) + Q_1^2 P_{12} + 2GQ_1(P_{11} + W_1 P_{12}) \tag{44}$$

$$T_1 = \int_0^1 U(1-\theta)\,d\eta = (1-\theta_b)(P_{13} + A P_{14}) - B(P_{15} + A P_{16} + W_p P_{17} + A W_p P_{18})$$

$$T_2 = \int_0^1 V(1-\theta)\,d\eta = (1-\theta_b)\left[G(P_{19} + W_1 P_{20}) + Q_1 P_{20}\right]$$

$$- B\left[G(P_{21} + W_p P_{22} + W_1 P_{23} + W_p W_1 P_{24}) + Q_1(P_{23} + W_p P_{24})\right]$$

and

$$M_1 = \int_0^1 \left(\frac{\rho_e}{\rho} - U\right) d\eta = \frac{H_e}{h_e} M_1^* + \left(\frac{H_e}{h_e} - 1\right)(M_{11} - M_{22})$$

$$M_1^* = \int_0^1 (\theta - U)\, d\eta = P_{25} - A P_{26} + \theta_b P_{27} + B\left(P_{28} + W_p P_{29}\right) \tag{44}$$

where the ideal-gas relationship

$$\frac{\rho_e}{\rho} - U^2 = \frac{H_e}{h_e}(\theta - U^2) - \left(\frac{H_e}{h_e} - 1\right) V^2$$

has been used. The coefficients, i.e., P_{ij}, are included in the Appendix.

II-C Integral Equations

Substitution of the profiles chosen in Sec. II-B into the integral equations (21), (22), and (23) yields

$$\frac{\partial \Omega^2}{e_1\, \partial(\phi/\ell)} + \frac{2\Omega^2}{e_1} \frac{\partial}{\partial(\phi/\ell)} \left[\ln \bar{\rho}_e M_{11} \bar{u}_e^{2 + \frac{M_1}{M_{11}}} E_2^{1 + \frac{M_{22}}{M_{11}}} \right] = \frac{2F_1}{M_{11}} (A + W)$$

$$+ \frac{2\Omega^2 M_2}{e_2 M_{11}} \frac{\partial \ln e_1 u_e}{\partial(\psi/\ell)} - \frac{2\Omega^2 M_{12}}{e_2 M_{11}} \frac{\partial \ln e_1 u_e^2 \bar{\rho}_e}{\partial(\psi/\ell)} - \frac{2\Omega}{M_{11}} \frac{\partial(\Omega M_{12} \sqrt{R_e}/\ell)}{e_2\, \partial(\psi/\ell)} \tag{45}$$

$$\frac{\partial(M_{21}\Omega)}{e_1\, \partial(\phi/\ell)} + \frac{M_{21}\Omega}{e_1} \frac{\partial\left[\ln \bar{\rho}_e \bar{u}_e^2 E_2^2\right]}{\partial(\phi/\ell)} = -D_1 \Omega (M_{11} + M_1) - \frac{F_1}{\Omega}\left(\frac{a^3 G - Q}{a^2 + W}\right)$$

$$- \frac{M_{22}\Omega}{e_2} \frac{\partial\left[\ln e_1 u_e^2 \bar{\rho}_e\right]}{\partial(\psi/\ell)} - \frac{1}{e_2} \frac{\partial(M_{22}\Omega)}{\partial(\psi/\ell)} \tag{46}$$

$$\frac{\partial(T_1\Omega)}{e_1\, \partial(\phi/\ell)} + \frac{T_1\Omega}{e_1} \frac{\partial\left[\ln \bar{\rho}_e \bar{u}_e E_2\right]}{\partial(\phi/\ell)} = \frac{F_1}{\Omega}\left(\frac{B}{Pr_b} + W\theta_b\right)$$

$$- \frac{T_2\Omega}{e_2} \frac{\partial\left[\ln e_1 u_e \bar{\rho}_e\right]}{\partial(\psi/\ell)} - \frac{1}{e_2} \frac{\partial(T_2\Omega)}{\partial(\psi/\ell)} \tag{47}$$

where

$$F_1 = \left(\frac{\rho_b}{\rho_e}\right) \frac{\bar{\mu}_b}{\bar{\rho}_e \bar{u}_e}$$

and x, y are replaced by ϕ and ψ, respectively. The term ψ takes on a physical meaning of stream function while ϕ can, in the case of irrotational outer flow, signify the velocity potential. Since the compatibility conditions have already been incorporated in Sec. II-B, they are not written here. Thus, there are three integral equations, and the parameters to be determined from these equations are Ω, G and B and the problem is mathematically determinate. Before discussing the method of solution, it is instructive to consider some special cases for which analyses are available.

CASE 1. Incompressible, No Mass Injection, Small Secondary Flow

This case has been analyzed previously by Cooke[18]. Under the conditions specified above, the present formulation, i.e., Eqs. (21) and (22), reduces to his equations by establishing the equivalence between the respective terms. The correspondence is as follows

Cooke's Formulation (Cooke's Notations)	Present Formulation (when specialized to Cooke's conditions)
σ	$\left(\frac{\rho_e}{\rho_b}\right)^2 \frac{1}{\nu_b} \left(\frac{\Delta}{a}\right)^2$
$2 + \Lambda$	A
π	G
M	$\frac{\rho_b}{\rho_e} F$
ρ_1	$(\epsilon_1 u_e)^{-\frac{1}{2}}$
ρ_2	$(\epsilon_2 u_e)^{-\frac{1}{2}}$

Cooke compares his results with the exact solutions of Hansen and Herzig[11] and obtains good agreement. Since the present formulation reduces to Cooke's formulation when specialized to his conditions, i.e., incompressible, no mass injection and small secondary flows, the present formulation will yield the same results as that of Cooke[18]. Zaat[15] earlier had considered the same case with the assumption that the inviscid outer flow is irrotational. In this case, the ϕ-lines are potential lines and, furthermore, $e_1 = u_e^{-1}$ (see Refs. 1, 2). The streamwise integral in the equation in this case becomes, in the present notations,

$$\frac{\partial}{\partial \phi}\left(e_2^2 u_e^6 \Delta^2\right) = 35.9\, e_2^2 u_e^4 \nu \tag{48}$$

and a simple quadrature is obtained for Δ, which is a measure of the boundary-layer thickness.

CASE 2. Incompressible, No Mass Injection, Axisymmetric Flow

This is a more specialized situation of Case 1 in that now there is no secondary flow. In this case, we may take the azimuth angle ψ in a circular section perpendicular to the axis as stream function. Then we have, for the line element,

$$(ds)^2 = \left(\frac{d\phi}{u_e}\right)^2 + (r\,d\psi)^2 \tag{49}$$

where r corresponds to the cylindrical radius from the axis of symmetry to the body surface. Comparison of Eqs. (1) and (49) gives

$$e_2 = r \tag{50}$$

Equation (48) then becomes

$$\frac{\Delta^2}{\nu} = \frac{35.9}{r^2 u_e^6} \int_0^X r^2 u_e^5\, dX \tag{51}$$

which is similar to Truckenbrodt's result[66]. The term X signifies the distance along a streamline.

CASE 3. Incompressible, No Mass Injection, Two-Dimensional Flow

In this case, we have, for the line element,

$$(ds)^2 = \left(\frac{d\phi}{u_e}\right)^2 + (d\psi)^2 \tag{52}$$

which gives, for potential flow,

$$e_2 = 1 \tag{53}$$

Hence, Eq. (48) becomes

$$\frac{\Delta^2}{\nu} = \frac{35.9}{u_e^6} \int_0^x u_e^5 \, dX \tag{54}$$

From Eqs. (20), (44), and the Appendix, we have

$$\theta_{11} = \Delta M_{11} = \Delta (0.1143 + 0.00953A - 0.00397A^2). \tag{55}$$

The range of interest for A is between 1 and 3, the value 2 corresponding to the "Blasius" case of flat-plate with no mass injection. Within this range, an average value for M_{11} yields $(M_{11})_{avg} = 0.115$. Substitution of this value in Eq. (54) gives

$$\frac{\theta_{11}^2}{\nu} = \frac{0.45}{u_e^6} \int_0^x u_e^5 \, dX \tag{56}$$

which agrees well with the results obtained by Tani[65] and Thwaites[47].

II-D Solutions and Discussion of Results

We now consider the method of solving the integral Eqs. (45), (46), and (47). From the inviscid flow-field analysis, the quantities at the outer edge of the boundary layer are assumed known, including the streamline curvature distribution (D_1) and the streamline divergence-convergence function (E_2). With known initial conditions, integration of the equations is then carried out along individual external streamlines (ψ = constant). The last term in each equation is of the form $\frac{\partial}{\partial \psi}\{\ \}$ and is not known a priori. Thus, this term is dropped at first[58, 67] and is accounted for after solutions have been obtained along several streamlines. It will be seen later in the

examples calculated that the saving in computation time, as well as simplicity of application, is achieved by this method. It should be remarked here that because only the gradient term is dropped at first, this method does not involve the assumption of small secondary flow, but rather is an iterative method of solving the equations.

As an application of the integral method formulated in Eqs. (45), (46), and (47), analysis will be made of a hypersonic flow around a blunt body at angle of attack with mass injection at the body surface assuming irrotational, inviscid outer flow and an ideal gas. Any other conditions or assumptions, such as the value of the Prandtl number, will be introduced as the analysis proceeds. From the condition of irrotational flow we get[1, 2]

$$e_1 = u_e^{-1} \tag{57}$$

and thus

$$K_1 = \frac{1}{e_1 e_2}\frac{\partial e_1}{\partial \psi} = \frac{-1}{u_e e_2}\frac{\partial u_e}{\partial \psi} \tag{58}$$

We shall now estimate the term $\partial \rho_e / \partial \psi$. Using ideal gas relationship, we obtain

$$\frac{1}{\rho_e}\frac{\partial \rho_e}{\partial \psi} = \frac{1}{p}\frac{\partial p}{\partial \psi} - \frac{1}{h_e}\frac{\partial h_e}{\partial \psi} \tag{59}$$

From Eq. (9), we have

$$\frac{\partial p}{\partial \psi} = e_2 K_1 \rho_e u_e^2 ,$$

and from the relationship $h_e = H_e - \frac{u_e^2}{2}$, we have, for H_e = constant,

$$\frac{\partial h_e}{\partial \psi} = -u_e \frac{\partial u_e}{\partial \psi} = e_2 K_1 u_e^2 \tag{60}$$

Combination of Eqs. (59), (9), and (60) yields the following result

$$\frac{1}{\rho_e e_2}\frac{\partial \rho_e}{\partial \psi} = K_1 \left(\frac{H_e}{h_e} - 1\right)\frac{2}{(\gamma-1)\gamma} = K_1 \beta \tag{61}$$

Thus, the transverse gradient of ρ_e may be conveniently expressed in terms of K_1. It is noted that near the stagnation point the term β is usually much less than unity and, thus, for air Eq. (61) is smaller than K_1.

Applying the relationships derived above in the integral equations (45), (46), and (47), we obtain

$$\frac{\partial(\Omega^2 F_2)}{\partial X} = \frac{2F_1F_2}{M_{11}}(A+W) + \frac{2(1-\beta)\Omega^2 D_1 F_2 M_{12}}{M_{11}} \tag{62}$$

$$\frac{\partial}{\partial X}(M_{21}\Omega F_3) = -F_3F_4 - \frac{F_1F_3}{\Omega}\left(\frac{a^3G-Q}{a^2+W}\right) \tag{63}$$

$$\frac{\partial}{\partial X}(T_1\Omega F_5) = \frac{F_1F_5}{\Omega}\left(\frac{B}{P_{r_b}} + W\theta_b\right) + \beta T_2 \Omega D_1 F_5 \tag{64}$$

where

$$\begin{aligned}
F_1 &= \left(\frac{\rho_b}{\rho_e}\right)\frac{\bar{\mu}_b}{\bar{\rho}_e\,\bar{u}_e} \\
F_2 &= \left[\bar{\rho}_e M_{11}\bar{u}_e^{\,2+\frac{M_1}{M_{11}}} E_2^{\,1+\frac{M_{22}}{M_{11}}}\right]^2 \\
F_3 &= \bar{\rho}_e\,\bar{u}_e^{\,2}E_2^{\,2} \\
F_4 &= \frac{H_e}{h_e} D_1\Omega\left[M_{11}+M_1^* - \left(1-\beta\frac{h_e}{H_e}\right)M_{22}\right] \\
F_5 &= \bar{\rho}_e\,\bar{u}_e E_2
\end{aligned} \tag{65}$$

and, as discussed previously, the last term in Eqs. (45), (46), and (47) has been dropped and will later be accounted for from the solutions obtained along the streamlines. A new variable X is introduced such that $dX = e_1 d\phi/\ell$, which signifies the length along the streamline. This is strictly for convenience in calculation, and no approximation is involved in this step[68]. From the inviscid outer flow field, distributions of the various terms, such as $\bar{\rho}_e$, D_1, $\bar{u}_e$, etc., are considered known. The dependent variables are

1. Ω , from which Δ, A, W, M_{11} can be calculated,
2. M_{21} , which in turn depends on G and Ω, and
3. T_1 , which will enable calculation for B .

Thus, there are three essential unknowns, Ω, G, and B . Since there are three equations, (62), (63), (64), the problem is now, mathematically speaking, solvable. Because of the complexity of the equations, numerical solution on a digital computer is carried out in the present analysis. Computation time for a typical case was about one minute on IBM 7044 computer.

In order to start the integration, it is necessary to know the initial values. If the integration were to start from an arbitrary point along the streamline, the initial conditions at that point are presumed given from the upstream conditions. However, if the integration starts from the stagnation point, the initial conditions can be determined from the integral equations themselves. Essentially, this involves dropping the slope terms for Ω^2, T_1, and M_{21} for the first approximation and then, by numerically differentiating these terms, obtain the second-order approximation, and the iteration is repeated until convergence in these values is achieved. Further details are included in Refs. 15 and 60. It has been repeatedly found by Cooke[18] that the main part of the solution is not sensitive to the way in which the solution is started. This conclusion was reinforced by Head[54] who used, as initial conditions, the Blasius velocity profile despite the fact that the pressure gradient at the initial point was not zero. He found that after a very short distance the solutions approached those obtained using the more elaborate, iterative technique. In the present analysis, both the iterative technique and an approximate technique have been tested for a specific problem. For the approximate technique, the initial values used were obtained by taking a limit of the Eqs. (62), (63), and (64) to the stagnation point. It was found that both techniques yielded equally reasonable results for the main part of the solution along the streamline and it was decided to apply the approximate technique in obtaining the initial conditions in the present analysis because of the saving in the computation time and simplicity in application.

Examples

The formulation derived in Eqs. (62), (63), and (64) will be applied to a flow on an Apollo-type blunt body entering the atmosphere. Specifically, the conditions assumed are:

Altitude: 200,000 ft

Velocity (u_∞): 30,000 ft/sec (0.915×10^6 cm/sec)

Body radius (ℓ): 15.5 ft (474 cm)

Angle of attack: 20 degrees

Under these conditions, the properties of equilibrium air behind a normal shock wave are,[69] in c.g.s. units

$$\frac{\rho_o}{\rho_\infty} = 16.81$$

$$\frac{p_o}{p_\infty} = 1099$$

$$\frac{T_o}{T_\infty} = 33$$

with

$$p_\infty = 2.26\ (10^2)\ [\text{dyne/cm}^2]$$

$$u_\infty = 0.915\ (10^6)\ [\text{cm/sec}]$$

$$\rho_\infty = 3.14\ (10^{-7})\ [\text{gr/cm}^3]$$

$$\mu_\infty = 1.6\ (10^{-4})\ [\text{gr/cm-sec}]$$

$$T_\infty = 2.5\ (10^2)\ [^\circ\text{K}]$$

$$Re_\infty = 8.8\ (10^5) = \rho_\infty u_\infty \ell/\mu_\infty$$

and

$$p_o = 2.49\ (10^5)\ [\text{dyne/cm}^2]$$

$$u_o = 5.45\ (10^4)\ [\text{cm/sec}]$$

$$\rho_o = 5.27\ (10^{-6})\ [\text{gr/cm}^3]$$

$$\mu_o = 0.916\ (10^{-3})\ [\text{gr/cm-sec}]$$

$$T_o = 8.25\ (10^3)\ [^\circ\text{K}]$$

$$Re = 1.44\ (10^5) = \rho_o u_o \ell/\mu_o$$

where $\mu_o/\mu_\infty \cong (T_o/T_\infty)^{1/2}$ was used across the normal shock. With these property values, the Eqs. (62), (63), and (64) were integrated along the streamline from the stagnation point assuming an ideal gas for cases of

arbitrarily chosen mass-injection rates, ranging from the solid-wall case, (N = 0), to a uniform 15 per cent injection rate (N = 0.15). Variable mass-injection fluxes along the streamline were also analyzed. In all the examples considered, the wall temperature was assumed constant at one-tenth of the free-stream stagnation temperature. The distributions along the streamline of $\mathcal{D}_1$, $\bar{u}_e$, $\bar{\rho}_e$, E_2, etc. were assumed expressible in analytic forms, e.g., $\bar{u}_e = \alpha_m X - \beta_m X^2$. This is strictly for convenience, since these distributions can be easily put on the digital computer in tabular forms or in curve-fit expressions. Specifically, the following distribution forms are assumed, in the present example, based on an inviscid analysis[70]:

$$
\begin{aligned}
\bar{u}_e &= 56.5\,X - 20\,X^2 \\
E_2 &= 1.0 - \exp(-15X) \\
\mathcal{D}_1 &= 30X\left\{\exp(-100X^2) - \frac{0.6}{X + 1.0}\right\} \\
\bar{\rho}_e &= 1.022 - 0.8\,X^2 \\
\bar{\rho}_b &= 10.22 \\
\bar{\mu}_b &= 0.1022 \\
\theta_b &= 0.10
\end{aligned}
\qquad (66)
$$

These distributions are shown in Fig. 11. The streamline curvature function $\mathcal{D}_1$ is expressed in the particular form shown in Eq. (66) in order to allow for the change in the sign of $\mathcal{D}_1$, $\mathcal{D}_1 = 0$ denoting the streamline inflection point, and the above appears to be a reasonable, general form. It should be noted in passing that the local radius of streamline curvature can be obtained simply as $\ell/\mathcal{D}_1$.

The results obtained are shown in Figs. 12 through 17. Figure 12 shows the distributions of Ω, the dimensionless "boundary-layer thickness" in the transformed plane, for various mass-injection rates. It is noted that Ω increases with increasing N, a physically reasonable result that has been obtained in previous analyses[16, 71]. It may also be seen from Fig. 12 that Ω, for large mass-injection rates, at first increases, then decreases along the streamline. This is due mainly to the second term in Eq. (62), containing $\mathcal{D}_1$ and Ω^2. Because, for increasing injection rates, Ω increases and because, in the present example, $\mathcal{D}_1$ is comparatively large far

downstream from the stagnation point, this term is seen to influence the magnitudes of the boundary-layer thickness along the streamline. When $\Delta = \Omega \ell/\sqrt{Re}$ is transformed back into the physical plane by the relationship $\delta = \int_0^{\Delta} \frac{\rho_e}{\rho} d\bar{z}$, with ρ_e decreasing with X and ρ_b held constant in the example, the thickening rate of δ is not as great as that of Δ. Thus, this demonstrates the greater sensitivity of Δ to the flow conditions in the transformed plane than in the actual physical plane, a useful result, enabling determination of the effects of various conditions in an exaggerated manner in the transformed plane.

Figures 13 and 14 describe the variations of the pressure-gradient parameter (P) and the mass-injection parameter (W) along the streamline. These are combined to yield the streamwise wall-shear parameter (A) from the relationship $A = (12 + P)/(6 + W)$. It may be seen that P and W exert opposite influences on the streamwise skin friction. The parameter A can be related to the physical streamwise wall-shear stress τ_{1b} by $A/\Delta = \tau_{1b}\, \rho_e/(\rho_b \mu_b u_e)$. Figure 15 shows the effects of various mass-injection rates on the streamwise wall shear. Consistent with previous analyses[16, 71], the results show lower values of wall shear for greater injection rates.

Figure 16 shows the results for the heat-transfer distribution along the streamline for various mass-injection rates. In particular, the heat-transfer parameter B may be related to the conventional heat-transfer term, i.e., Nusselt number, by $B/\Delta = Nu\left(\frac{h_e}{H_e} - \theta_b\right)\rho_e/(\rho_b \ell)$. It shows that the heat-transfer rate decreases for increasing injection rates and, at uniform 15 per cent mass flux at the wall, the heat transfer rate is practically zero, signifying a nearly-insulated condition. It is noted that the decrease in B with increasing mass-injection rate is greater than that of A, so that for a certain value of mass flux, the body may be practically insulated, while there is still a finite skin friction. This result was also obtained in a previous analysis in Ref. 16.

Figure 17 describes the distribution of the transverse wall-shear stress along the streamline. Also shown in the figure is the prescribed streamline curvature distribution D_1, which goes through zero, i.e.,

inflection point, at $X \cong 0.076$ corresponding to a distance of 36 cm. from the stagnation point in the present example. It is seen that $\mathcal{D}_1$ is at first increasing and then becomes negative, while the wall shear is negative and later becomes positive. This is a reasonable result, since it follows from Eq. (9) that $\mathcal{D}_1 = K_1 \ell$ and the transverse pressure gradient $\frac{\partial p}{e_1 \partial y}$ have the same sign. Since the transverse-(or secondary flow) velocity component is in the direction of lower pressure, this means that v and $\frac{\partial p}{e_1 \partial y}$ possess opposite signs. The results in Fig. 17 confirm this conclusion. An interesting result is noted immediately after the inflection point in the figure where C (denoting the direction of v near the wall) and $\mathcal{D}_1$ (and thus $\frac{\partial p}{e_1 \partial y}$) both have the same signs. This signifies the nonsimilarity effect of the flow taken into account in the present analysis, where the influence of the upstream momentum is still present at the inflection point. After some distance beyond the inflection point, this flow sufficiently adjusts to the change in the streamline curvature $\mathcal{D}_1$, so that v and $\mathcal{D}_1$ again possess opposite signs. This result was also observed by Cooke[18] in his approximate analysis and by Hansen and Herzig[11] in their exact solutions for the incompressible, solid-wall case. Thus, the present analysis describes the nonsimilar effects of the inflection point on the flow even in the case of mass injection.

Another interesting result is observed in Fig. 17B where increased mass-injection rates bring about decrease in the distance between the streamline inflection point and the point at which the secondary flow reverses its direction, so that the two points virtually coincide for uniform 15% injection rate. Physically, this signifies that the lower-velocity mass being injected into the flow responds more quickly to the change in the streamline curvature than the outer fluid.

As in the results for the streamwise flow and the total enthalpy, the magnitude of the transverse velocity gradient at the wall, i.e., the transverse wall shear, decreases with increasing mass-injection rates. The angle between the inviscid external streamline and the limiting streamline at the body surface may be determined from the relationship

$$\alpha = \tan^{-1}\left(\frac{C}{A}\right) \tag{67}$$

Figures 15 and 17 show that the absolute magnitude of α increases with increasing mass-injection rate, a result obtained due to a slower decrease in C compared to a more sensitive change in A with increasing mass flux. Thus, the limiting streamlines tend to diverge more with mass injection than without, exhibiting greater three-dimensionality of the flow. This result has also been obtained in a previous analysis[16] where small secondary flow was assumed. It is to be noted that α reaches a certain finite value as mass-injection rate is further increased, signifying that the surface streamline has a limiting angle with the outer inviscid streamline in the case of very large mass-injection rates. This is due to the fact that both A and C vary only slightly as N becomes very large.

Comparisons will now be made with other solutions for Δ, the boundary-layer thickness, and A, the shear-stress parameter in the streamwise direction. In particular, the values at the stagnation point will be compared. Using the Howarth-Dorodnitzyn similarity transformation[72], i.e.,

$$\xi = \int_0^s \rho_b \mu_b u_e r_b^2 \, ds$$

$$\eta^* = \frac{\rho_e u_e r_b}{\sqrt{2\xi}} \int_0^z \frac{\rho}{\rho_e} \, dz \tag{68}$$

and Eq. (16), we obtain

$$\eta_e^* = \frac{\rho_e u_e r_b}{\sqrt{2\xi}} \Delta \tag{69}$$

In the stagnation region, we may use approximately $r_b \sim s$, $u_e \sim \left(\frac{\partial u_e}{\partial s}\right)_{s=0} s$. Hence, Eq. (69) becomes

$$\eta_e^* \cong \Delta \left(\frac{2 \rho_e^2 \left(\frac{\partial u_e}{\partial s}\right)_{s=0}}{\rho_b \mu_b} \right)^{1/2} \tag{70}$$

For the example used in the present analysis, the value of the square-root quantity in Eq. (70) is approximately 2.80. Now, from the results, Δ for $N = 0$ is 1.20 at the stagnation point, while $\Delta \cong 2.1$ for $N = 0.01$.

On the other hand, the similarity solution obtained in Ref. 16 gives, for $\theta_b = 0.1$ and $\beta^* = \frac{2\xi}{u_e}\frac{H_e}{h_e}\frac{\partial u_e}{\partial \xi} = 0.5$, $\eta_e^* \cong 3.30$ for $f_b = 0$ $(N = 0)$, and $\eta_e^* \cong 6.0$ for $f_b = -0.5$ $(N \cong 0.01)$. It is thus demonstrated from Eq. (70) that the results for Δ obtained in the present analysis are reasonable.

We shall now compare the streamwise wall-shear parameter, which is termed A in the present analysis and its corresponding quantity is usually called f_b'' in the similarity analyses. Specifically, we wish to determine the actual streamwise skin friction defined to be $\tau_{1b} = \mu_b (\partial u/\partial z)_b$. In the present formulation, τ_{1b} is expressible to be

$$\tau_{1b} = \frac{\rho_b u_e \mu_b}{\rho_e \Delta} A \tag{71}$$

while similarity transformation of Howarth-Dorodnitzyn gives, from Eq. (69)

$$\tau_{1b} = \frac{\mu_b \rho_b u_e r_b u_e}{\sqrt{2\xi}} f_b'' = \frac{\mu_b \rho_b u_e}{\rho_e \Delta} \eta_e^* f_b'' \tag{72}$$

Thus, from Eqs. (71) and (72), the comparison to be made is between A and $\eta_e^* f_b''$. The case of zero pressure gradient and zero mass injection gives $P = 0$ and $N = 0$, and therefore A is identically 2.0. On the other hand, from similarity analysis, this case corresponds to $f_b = 0$ (no mass injection) and $\beta^* = 0$ (zero pressure gradient). From Ref. 73, we obtain $\eta_e^* \cong 4.20$, $f_b'' \cong 0.47$, and hence $\eta_e^* f_b'' \cong 1.98$, which is close to 2.0, a value for A obtained from the present analysis. The mass injection case will now be compared. Specifically, 5% injection rate, i.e., $N = 0.05$ gives, at the stagnation point, $A \cong 0.27$, while, from similarity analysis,[16] $\eta_e^* \cong 11.0$ and $f_b'' = 0.025$, and hence $\eta_e^* f_b'' = 0.275$ for $\beta^* = 0.5$ and $\theta_b = 0.1$, confirming the reasonableness of the results obtained in the present analysis.

It is thus shown that solutions can be obtained along any streamline based on the integral method formulated in the present analysis. After calculations have been obtained along several streamlines, the suppressed terms, viz., $\frac{\partial}{\partial \psi}\{\ \}$, in Eqs. (45), (46), and (47) can be determined, and, if these

terms are not small compared to other terms in the equations, the calculations can be performed once more along the streamlines until convergence is reached. This has not been carried out in the present analysis, since this type of iterative procedure has proved to be successful and reasonable[58,67,74] and since the conditions in the present examples were rather arbitrarily assigned in order to test the applicability of the integral method.

Finally, it is to be remarked that the present formulation should be extendable to the case of dissociated flow. It will require assuming a suitable form for the species profiles, and the modification of the definition of M_1 and other property terms. Thus, simultaneous integration of the equations along the streamlines should yield approximate, nonsimilar solutions for the flow characteristics, including the species concentrations.

CONCLUSIONS

An analysis of nonsimilar, three-dimensional, compressible, laminar boundary layers with mass injection has been formulated by employing the integral method. Comparisons were made with other analyses performed for specialized cases such as incompressible, solid-wall, or small secondary (transverse) flows, and the present formulation was found to be in good agreement. As an application of the formulation, sample solutions were performed for the forebody flow on a blunt body with variable mass-injection rates. The results demonstrate significant influences of mass injection and the streamline curvature changes on the flow characteristics, such as decrease in the shear stresses and the heat transfer with increase in mass flux; these results are consistent with other, more specialized analyses.

REFERENCES

1. Cooke, J. C. and Hall, M. G., Boundary Layers in Three Dimensions. Section in Progress in Aeronautical Sciences, Vol. 2, Pergamon Press, 1962, pp. 221-282. Edited by A. Ferri, D. Kuchemann, and L. Sterne.

2. Mager, A., Three-Dimensional Laminar Boundary Layers. Section C in Theory of Laminar Flows, High-Speed Aerodynamics and Jet Propulsion, Vol. IV, pp. 286-394. Edited by F. K. Moore, Princeton 1954

3. Moore, F. K., Three-Dimensional Boundary Layer Theory. Advances in Applied Mechanics, Vol. IV, pp. 159-228, Academic Press, 1956

4. Rosenhead, L. (ed.) Laminar Boundary Layer. Clarendon Press, Oxford, 1963

5. Reshotko, E., Heat Transfer to a Yawed Infinite Cylinder in Compressible Flow. 1956 Heat Transfer and Fluid Mechanics Institute, Stanford, Calif., p. 205

6. Tinkler, J., Effect of Yaw on the Compressible Laminar Boundary Layer. ARC, R & M 3005 (1957)

7. Reshotko, E. and Beckwith, I. E., Compressible Laminar Boundary Layers Over a Yawed Infinite Cylinder with Heat Transfer and Arbitrary Prandtl Number. NACA TN 3986 (1957)

8. Mager, A. and Hansen, A. G., Laminar Boundary Layer Over a Flat Plate in a Flow Having Circular Streamlines. NACA TN 2658 (1952)

9. Sowerby, L., Secondary Flow in a Boundary Layer. RAE Rept No. Aero 2512 (March 1954)

10. Loos, H. G., A Simple Laminar Boundary Layer with Secondary Flow. J. Aero. Sci. 22, 1, pp. 35-40 (1955)

11. Hansen, A. G. and Herzig, H. Z., Cross Flows in Laminar Incompressible Boundary Layers. NACA TN 3651 (1956)

12. Vaglio-Laurin, R., Laminar Heat Transfer on Three-Dimensional Blunt-Nosed Bodies in Hypersonic Flow. ARS J. 29, pp. 123-129 (Feb. 1959)

13. Eichelbrenner, E. and Oudart, A., Methode de Calcul de la Couche Limite Tridimensionnelle. Application a un Corps Fuselé Incliné sur le Vent. O. N. E. R. A. Publ. No. 76 (1955)

REFERENCES (Cont.)

14. Mager, A., Three-Dimensional Laminar Boundary Layer with Small Cross-Flow. J. Aero. Sci., 21, pp. 835-845 (1954)

15. Zaat, J. A., A Simplified Method for the Calculation of Three-Dimensional Laminar Boundary Layers. NLL Report F. 184 (1956)

16. Kang, S. W., Rae, W. J., and Dunn, M. G., Effects of Mass Injection on Compressible, Three-Dimensional, Laminar Boundary Layers with Small Secondary Flow. CAL Report No. AI-2187-A-2 (Aug. 1966)

17. Cooke, J. C., An Axially Symmetric Analogue for General Three-Dimensional Boundary Layers. ARC, R & M No. 3200 (June 1959)

18. Cooke, J. C., Approximate Calculation of Three-Dimensional Laminar Boundary Layers. RAE Rept No. Aero 2658 (1959)

19. Beckwith, I. E., Similarity Solutions for Small Cross Flows in Laminar Compressible Boundary Layers. NASA TR R-107 (1961)

20. Chan, Y. Y., An Approximate Method for Three-Dimensional Compressible Laminar Boundary Layers with Small Cross-Flow. NRC Aero. Rept. LR-455 (1966)

21. Fannelop, T. K., A Method of Solving the Three-Dimensional Laminar Boundary-Layer Equations with Application to a Lifting Reentry Body. AVCO Rept. AVMSD-0209-66-RM (1966)

22. Tsen, L. F., Contribution a l'étude de la Couche Limite Tridimensionelle Laminaire Compressible Avec Transfert de Chaleur (a Dissertation) De L'université de Poitiers, France, 1965

23. Howarth, L., The Boundary Layer in Three-Dimensional Flow. Part II - The Flow Near a Stagnation Point. Phil. Mag. (7) 42, pp. 1433-1440 (1951)

24. Davey, A., Boundary-Layer Flow at a Saddle Point of Attachment. J. Fluid Mech. 10, pp. 593-610 (1961)

25. Poots, G., Compressible Laminar Boundary-Layer Flow at a Point of Attachment. J. Fluid Mech. 22, pp. 197-208 (1965)

26. Libby, P. A., Heat and Mass Transfer at a General Three-Dimensional Stagnation Point, AIAA J. 5, pp. 507-517 (1967)

27. Hayes, W. D., The Three-Dimensional Boundary Layer. NAVORD Rept. 1313 (China Lake, Calif.) (1951)

28. Hansen, A. G. and Herzig, H. Z., On Possible Similarity Solutions for Three-Dimensional Incompressible Laminar Boundary Layers. I - Similarity with Respect to Stationary Rectangular Coordinates. NACA TN 3768 (1956)

29. Herzig, H. Z. and Hansen, A. G., On Possible Similarity Solutions for Three-Dimensional Incompressible Laminar Boundary Layers. II - Similarity with Respect to Stationary Polar Coordinates. NACA TN 3832 (1956)

30. Herzig, H. Z. and Hansen, A. G., On Possible Similarity Solutions for Three-Dimensional Incompressible Laminar Boundary Layers. III - Similarity with Respect to Stationary Polar Coordinates for Small Angle Variation. NACA TN 3890 (1957)

31. Hansen, A. G., On Possible Similarity Solutions for Three-Dimensional Incompressible Laminar Boundary-Layer Flows Over Developable Surfaces and with Proportional Mainstream Velocity Components. NACA TM 1437 (1958)

32. Hansen, A. G. and Herzig, H. Z., Approximate Solutions of a Class of Similarity Equations for Three-Dimensional, Laminar, Incompressible Boundary-Layer Flows. NACA TN 4375 (1958)

33. Poots, G., A Solution of the Compressible Laminar Boundary Layer Equations with Heat Transfer and Adverse Pressure Gradient. Quart. J. Mech. and Appl. Math., 13, pp. 57-84 (1960)

34. Libby, P. A. and Pallone, A., A Method for Analyzing the Heat-Insulating Properties of the Laminar Compressible Boundary Layer. J. Aero. Sci., 21, pp. 825-834 (1954)

35. Libby, P. A. and Morduchow, M., Method for Calculation of Compressible Laminar Boundary Layer with Axial Pressure Gradient and Heat Transfer. NACA TN 3157 (1954)

36. Young, A. D., The Calculation of the Profile Drag of Aerofoils and Bodies of Revolution at Supersonic Speeds. Coll. Aero. Rept. No. 73, ARC 15970 (1953)

37. Eckert, E. R. G., Engineering Relations for Friction and Heat Transfer to Surfaces in High Velocity Flow. J. Aero. Sci. 22, 8, pp. 585 (1955)

38. Braun, W. H., Turbulent Boundary Layer on a Yawed Cone. NACA TN 4208 (January 1958)

39. Cooke, J. C., A Calculation Method for Three-Dimensional Turbulent Boundary Layers. RAE Rept. Aero. 2576 (1958)

40. Hall, M. G. and Dickens, H. B., Measurements in a Three-Dimensional Turbulent Boundary Layer in Supersonic Flow. RAE TR 66214 (July 1966)

41. Spence, D. A., The Growth of Compressible Turbulent Boundary Layers on Isothermal and Adiabatic Walls, ARC 21144, R&M 3191 (June 1959)

42. Pohlhausen, K., Zur näherungsweisen Integration der Differentialgleichung der laminaren Reibungsschicht, ZAMM, 1, 252 (1921)

43. Morduchow, M., On Heat Transfer Over a Sweat-Cooled Surface in Laminar Compressible Flow with a Pressure Gradient. J. Aero. Sci., 19, pp. 705-712 (1952)

44. Shanebrook, J. R. and Eichelbrenner, E. A., An Approximate Method of Treating the Three-Dimensional, Laminar, Incompressible Boundary-Layer Equations When the Cross Flow is Small. ASME Paper No. 66-WA/FE-34 (1966)

45. Libby, P. A., Morduchow, M., and Bloom, M., Critical Study of Integral Methods in Compressible Laminar Boundary Layers. NACA TN 2655 (1952)

46. Tien, C. L. and Gee, C., Hypersonic Viscous Flow Over a Sweat-Cooled Flat Plate. AIAA J. 1, pp. 159-167 (1963)

47. Thwaites, B., Approximate Calculation of the Laminar Boundary Layer. Aero. Quart. 1, Part III, Roy. Aero. Soc., London, pp. 245-280 (Nov. 1949)

48. Cohen, C. B. and Reshotko, E., The Compressible Laminar Boundary Layer with Heat Transfer and Arbitrary Pressure Gradient. NACA Rept. 1294 (1956)

49. Chan, Y. Y., Integral Methods in Compressible Laminar Boundary Layers and Their Application to Hypersonic Pressure Gradients. Univ. of Toronto UTIAS Rept. No. 104 (1965)

50. Timman, R. A., A One-Parameter Method for the Calculation of Laminar Boundary Layers. NLL Rept. F35 (1949)

51. Pallone, A., Nonsimilar Solutions of the Compressible Laminar Boundary Layer Equations with Applications to the Upstream-Transpiration Cooling Problem. J. Aero. Sci., 28, pp. 449-456 (1961)

52. Launder, B. E., An Improved Pohlhausen-Type Method of Calculating the Two-Dimensional Laminar Boundary Layer in a Pressure Gradient, J. Heat Transfer, ASME, 86, Sec. 3, No. 3, pp. 360-364 (1964)

53. Pallone, A., Moore, J. A., and Erdos, J. I., Nonequilibrium, Nonsimilar Solution of the Laminar Boundary-Layer Equations. AIAA J. 2, pp. 1706-1713 (1964)

54. Head, M. R., An Approximate Method of Calculating the Laminar Boundary Layer in Two-Dimensional Incompressible Flow. ARC, R&M 3123 (March 1957)

55. Head, M. R., Approximate Methods of Calculating the Two-Dimensional Laminar Boundary Layer with Suction. Section in Boundary Layer and Flow Control, Vol. 2, Pergamon (1961). Edited by G. Lachmann.

56. Cooke, J. C., Pohlhausen's Method for Three-Dimensional Laminar Boundary Layers. Aero. Quart., 3, 51 (1951)

57. Mager, A., Generalization of Boundary-Layer Momentum-Integral Equations to Three-Dimensional Flows Including Those of Rotating System. NACA Rept. 1067 (1952)

58. Lindfield, A. W., Pinsent, H. G., and Pinsent, P. A., Approximate Methods for Calculating Three-Dimensional Boundary Layer Flow on Wings. Boundary Layer and Flow Control, edited by G. V. Lachmann, Pergamon Press, London (1961)

59. Timman, R. A., Calculation Method for Three-Dimensional Laminar Boundary Layers, NLL Report F. 66 (1950)

60. Zaat, J. A., van Spiegel, E., and Timman, R., The Three-Dimensional Laminar Boundary Layer Flow About a Yawed Ellipsoid at Zero Incidence. NLL Rept. F. 165 (1955)

61. Cooke, J. C., Approximate Calculation of Three-Dimensional Laminar Boundary Layers. ARC, R&M 3201 (October 1959)

62. Liu, S. W. and Kuby, G. H., Interaction of Surface Chemistry and Mass Transfer in Nonsimilar Boundary-Layer Flows. AIAA J. 5, pp. 526-534 (1967)

63. Timman, R., The Theory of Three-Dimensional Boundary Layers. Symposium on Boundary Layer Effects in Aerodynamics, National Physical Laboratory (1955)

64. Timman, R. and Zaat, J. A., Eine Rechenmethode fur dreidimensionale laminaren Grenzschichten. 50 Jahre Grenzschichtforschung (1955), Friedr. Vieweg. u. Sohn Braunschweig.

65. Tani, I., On the Approximate Solution of the Laminar Boundary-Layer Equations. J. Aero. Sci., 21, pp. 487-495 (1954)

66. Truckenbrodt, E., Ein Quadraturverfahren zur Berechnung der laminaren und turbulenten Reibungsschicht bei ebener und rotationssymmetrischer Strömung., Ing. Arch., 20, 14, pp. 211-228 (1952)

67. Eichelbrenner, E. A., La Couche Limite Tridimensionnelle en Régime Turbulent d'un Fluide Compressible: Cas de la Paroi Athermale. AGARD Specialists' Meeting, Part 2, pp. 795-828 , Naples, Italy (May 1965)

68. Stewartson, K., The Theory of Laminar Boundary Layers in Compressible Fluids. Clarendon Press, Oxford, p. 118, (1964)

69. Marrone, P. V., Normal Shock Waves in Air: Equilibrium Composition and Flow Parameters for Velocities from 26, 000 to 50, 000 ft/sec. CAL Rept. AG-1729-A-2 (1962)

70. Bohachevsky, I. O. and Mates, R. E., A Direct Method for Calculation of the Flow about an Axisymmetric Blunt Body at Angle of Attack. AIAA J. 4, pp. 776-782 (1966)

71. Libby, P. A., The Homogeneous Boundary Layer at an Axisymmetric Stagnation Point with Large Rates of Injection. J. Aero. Sci. 29, pp. 48-60 (1962)

72. Hayes, W. D. and Probstein, R. F., Hypersonic Flow Theory. Academic Press, New York, 1959

73. Cohen, C. B. and Reshotko, E., Similar Solutions for the Compressible Laminar Boundary Layer with Heat Transfer and Pressure Gradient. NACA Rept. 1293 (1956)

74. Cumpsty, N. A. and Head, M. R., The Calculation of Three-Dimensional Turbulent Boundary Layers - (1) Flow Over the Rear of an Infinite Swept Wing. ARC 27680 (1966)

APPENDIX

From Eqs. (31), (36), and (38), we have

$$m_1(\eta) = \eta^2 (6 - 8\eta + 3\eta^2)$$

$$m_2(\eta) = \eta (1-\eta)^3$$

$$m_3(\eta) = \frac{\eta^2}{2} (1-\eta)^3$$

$$m_4(\eta) = \eta (1 - m_1)$$

$$m_5(\eta) = \eta^3 (10 - 15\eta + 6\eta^2)$$

$$g(\eta) = \frac{1}{2} \left[\operatorname{erfc}(a\eta) + (\eta - 1) e^{-a^2\eta^2} \right]$$

$$k(\eta) = a\eta e^{-a^2\eta^2}$$

where

$$a = \frac{3\sqrt{\pi}}{2}$$

Then we have,

$$P_1 = \int_0^1 (1 - m_1)\, m_1\, d\eta = 0.114286$$

$$P_2 = \int_0^1 (1 - 2m_1)\, m_2\, d\eta = +0.00953$$

$$P_3 = \int_0^1 m_2^2\, d\eta = 0.00396825$$

$$P_4 = \int_0^1 k\, m_1\, d\eta = 0.0756331$$

$$P_5 = \int_0^1 k\, m_2\, d\eta = 0.015252$$

$$P_6 = \int_0^1 g\, m_1\, d\eta = -0.0064069$$

$$P_7 = \int_0^1 g\, m_2\, d\eta = -0.0021876$$

$$P_8 = \int_0^1 k\, d\eta = 0.187903$$

$$P_9 = \int_0^1 g\, d\eta = -0.0252027$$

$$P_{10} = \int_0^1 k^2\, d\eta = 0.0589253$$

$$P_{11} = \int_0^1 k g\, d\eta = -0.0083928$$

$$P_{12} = \int_0^1 g^2 \, d\eta = 0.0014283$$

$$P_{13} = \int_0^1 m_1 (1 - m_5) \, d\eta = 0.169047$$

$$P_{14} = \int_0^1 m_2 (1 - m_5) \, d\eta = 0.036905$$

$$P_{15} = \int_0^1 m_1 m_4 \, d\eta = 0.047619$$

$$P_{16} = \int_0^1 m_2 m_4 \, d\eta = 0.0075397$$

$$P_{17} = \int_0^1 m_1 m_3 \, d\eta = 0.0045635$$

$$P_{18} = \int_0^1 m_2 m_3 \, d\eta = 0.00059524$$

$$P_{19} = \int_0^1 (1 - m_5) k \, d\eta = 0.139727$$

$$P_{20} = \int_0^1 (1 - m_5) g \, d\eta = -0.0219595$$

$$P_{21} = \int_0^1 m_4 k \, d\eta = 0.0289805$$

$$P_{22} = \int_0^1 m_3 k \, d\eta = 0.00228809$$

$P_{23} = \int_0^1 m_4 g \, d\eta = -0.0037695$

$P_{24} = \int_0^1 m_3 g \, d\eta = -0.00026364$

$P_{25} = \int_0^1 (m_5 - m_1) \, d\eta = -0.1$

$P_{26} = \int_0^1 m_2 \, d\eta = 0.050$

$P_{27} = \int_0^1 (1 - m_5) \, d\eta = 0.50$

$P_{28} = \int_0^1 m_4 \, d\eta = 0.10$

$P_{29} = \int_0^1 m_3 \, d\eta = 0.008333$

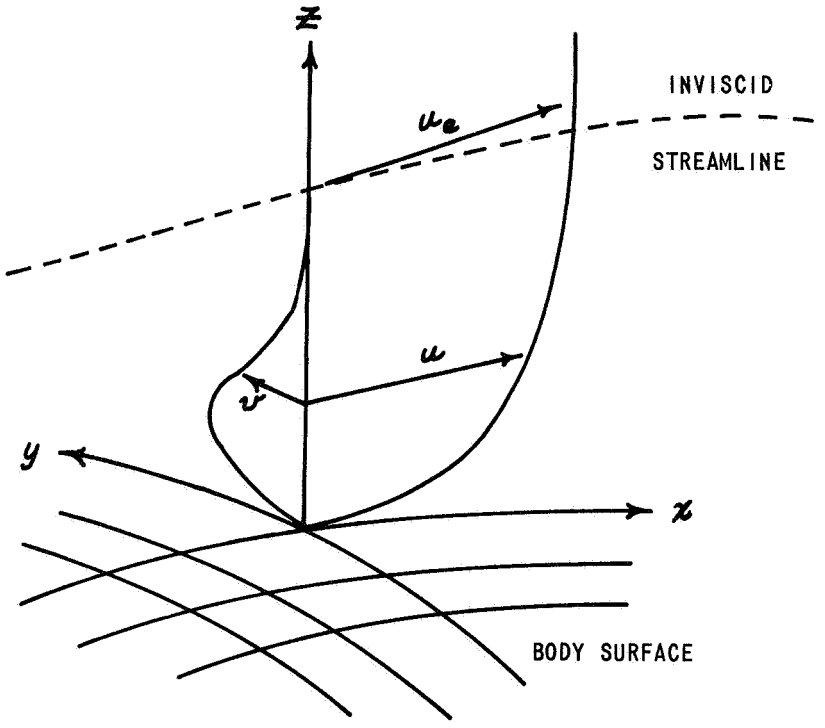

Figure 1 CO-ORDINATE SYSTEM

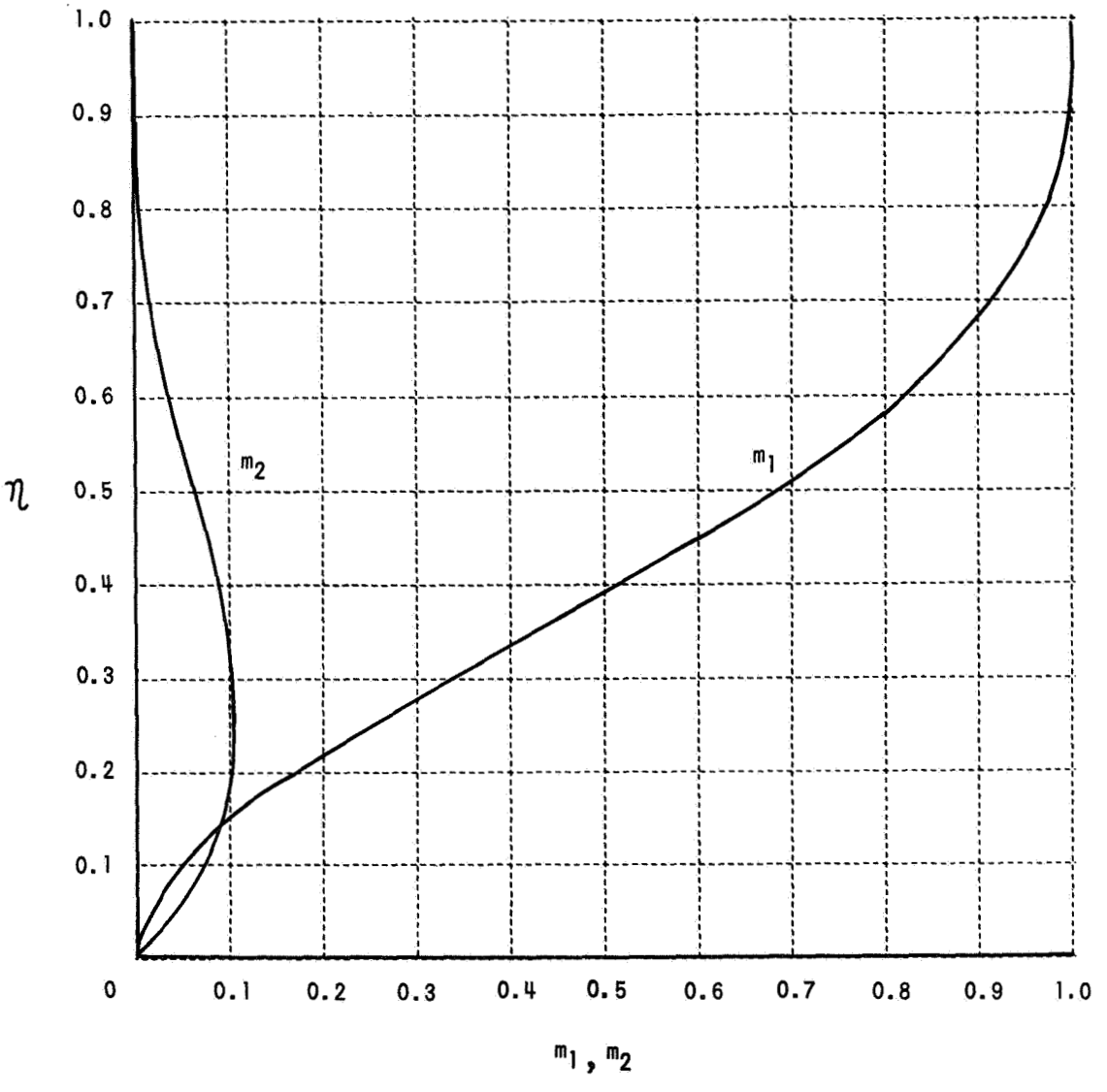

Figure 2 FUNCTIONS FOR THE STREAMWISE VELOCITY PROFILE

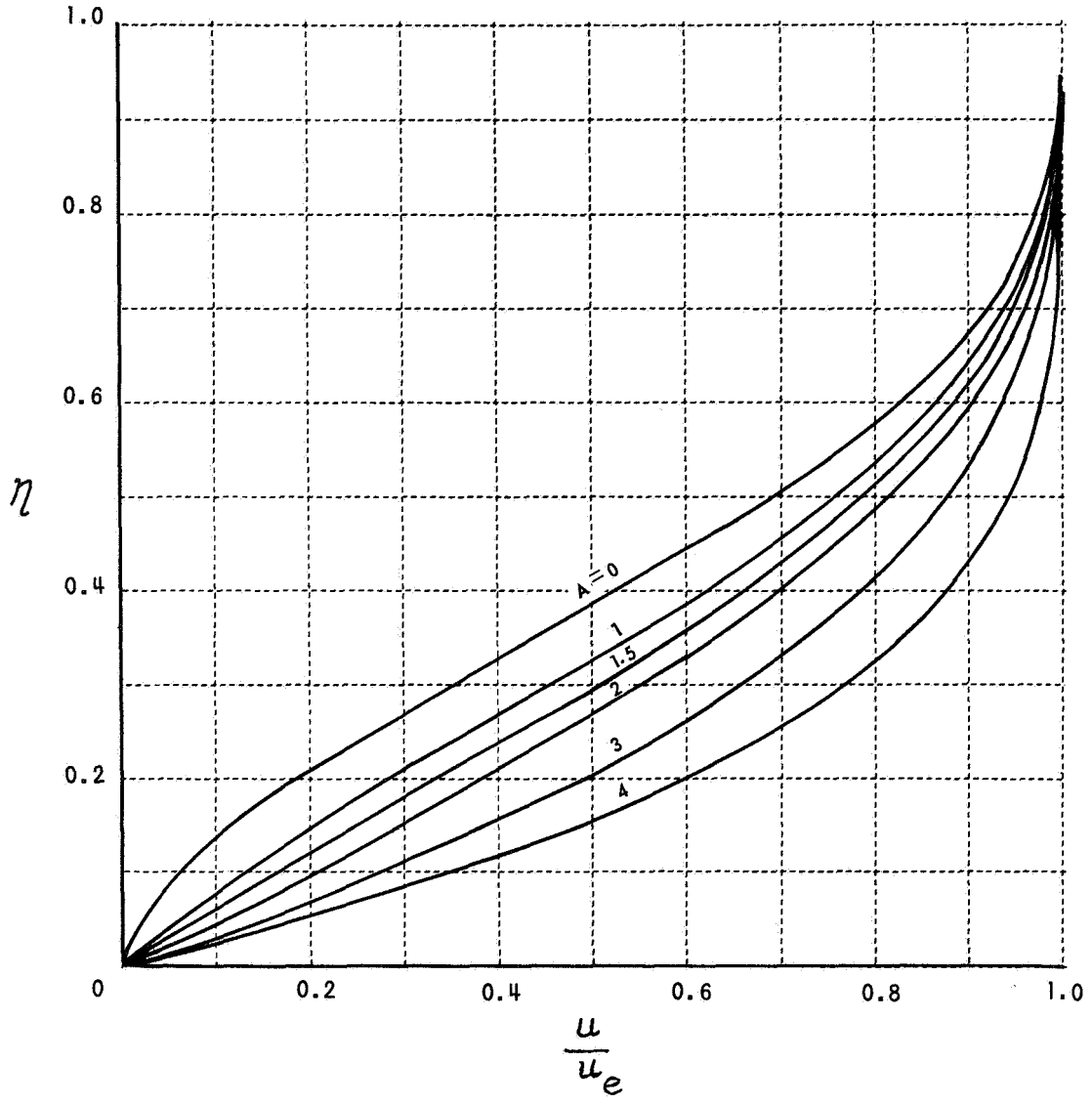

Figure 3 DISTRIBUTIONS OF THE STREAMWISE VELOCITY PROFILES

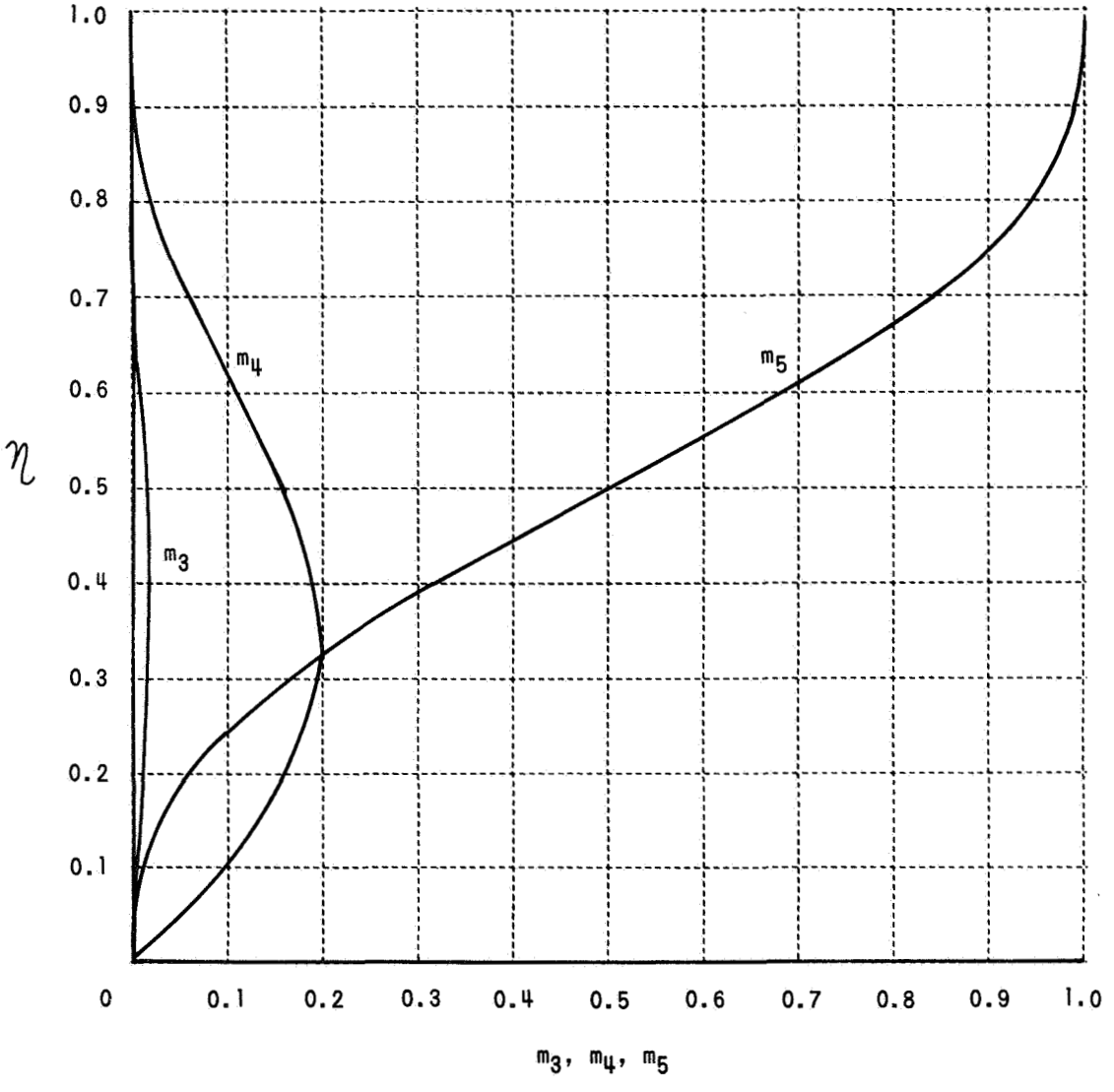

Figure 4 FUNCTIONS FOR THE TOTAL - ENTHALPY PROFILE

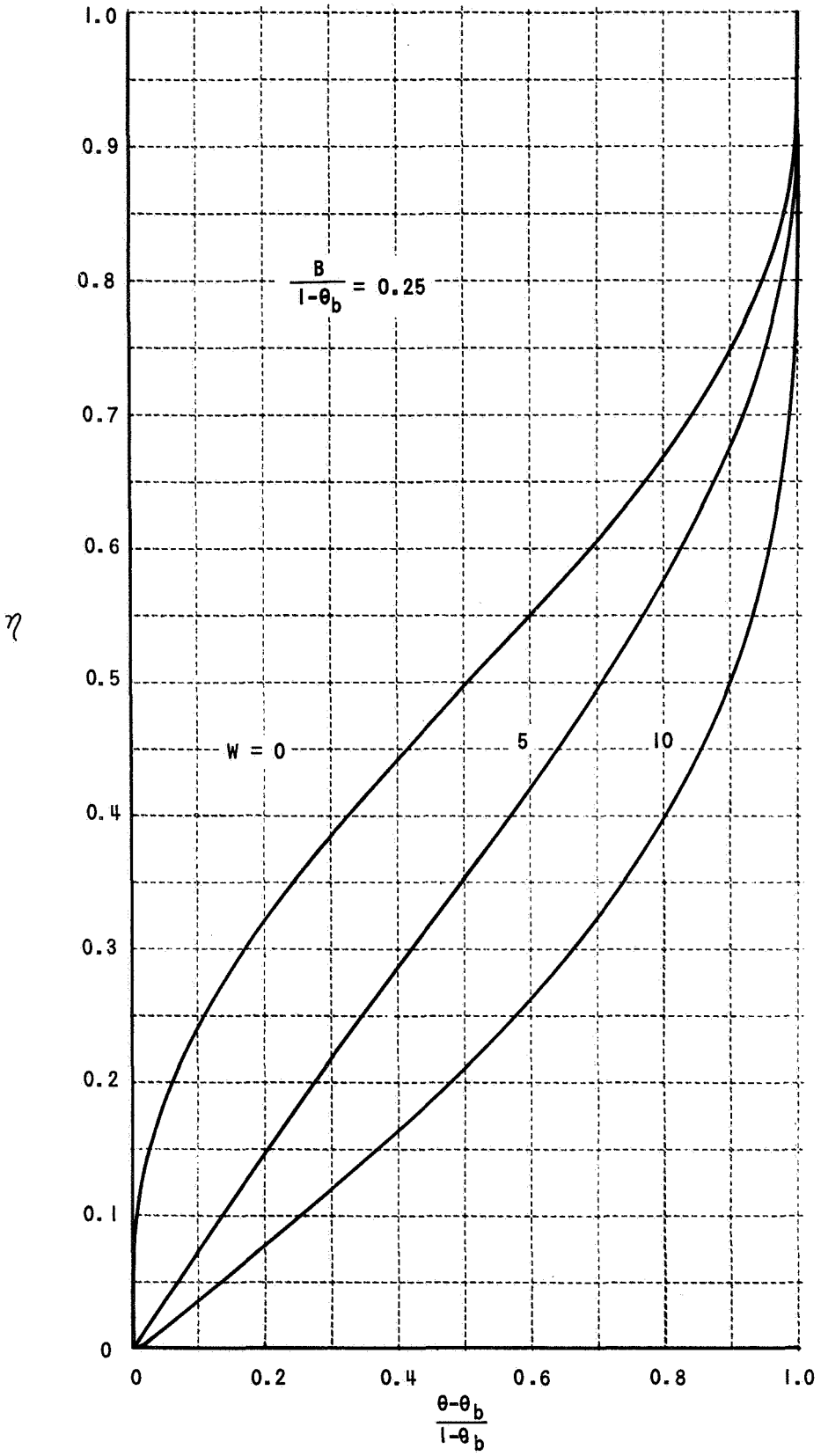

Figure 5 DISTRIBUTIONS OF TOTAL - ENTHALPY PROFILES

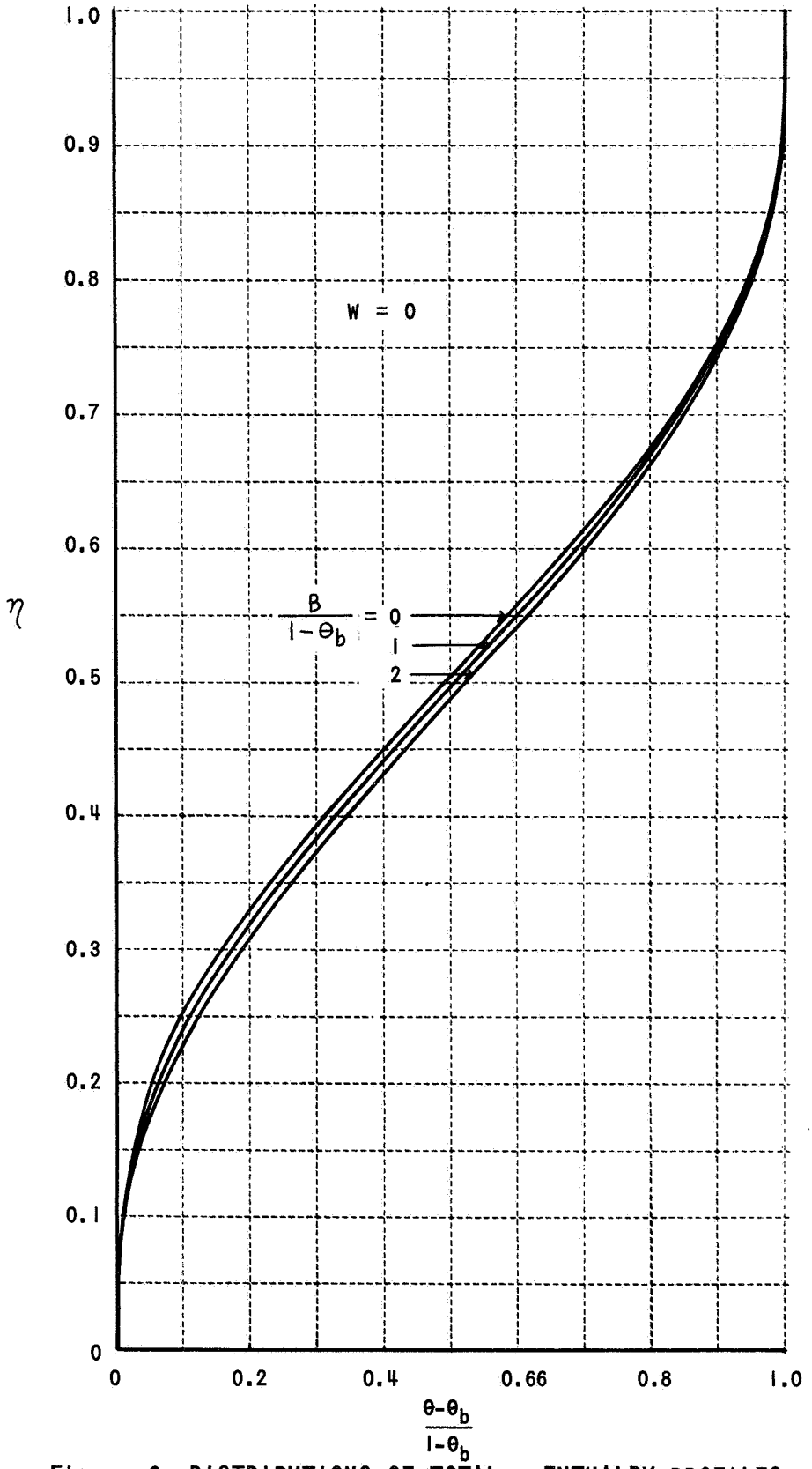

Figure 6 DISTRIBUTIONS OF TOTAL - ENTHALPY PROFILES

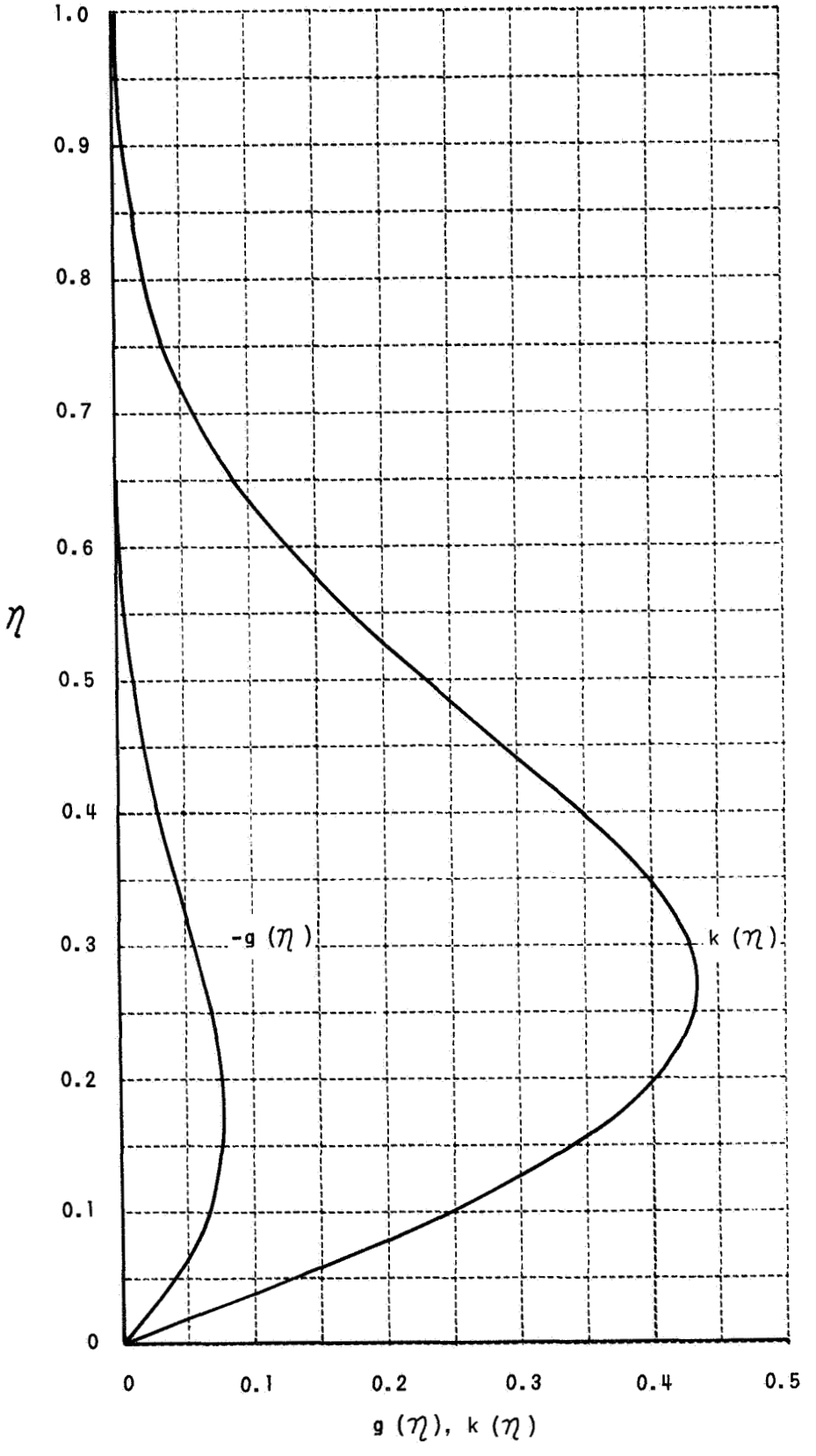

Figure 7 FUNCTIONS FOR THE SECONDARY - FLOW VELOCITY PROFILE

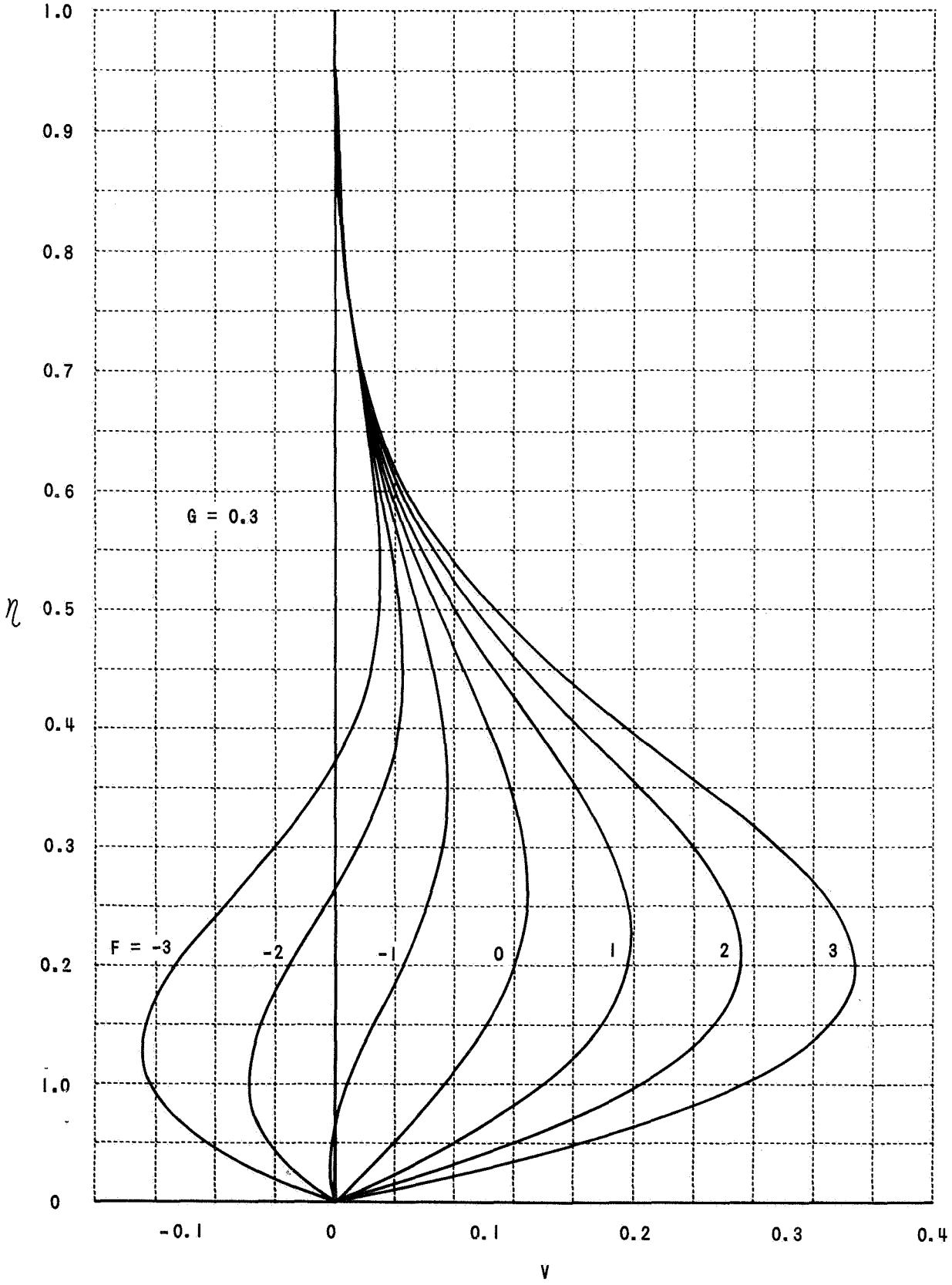

Figure 8 DISTRIBUTIONS OF THE SECONDARY-FLOW VELOCITY PROFILES (G = 0.3)

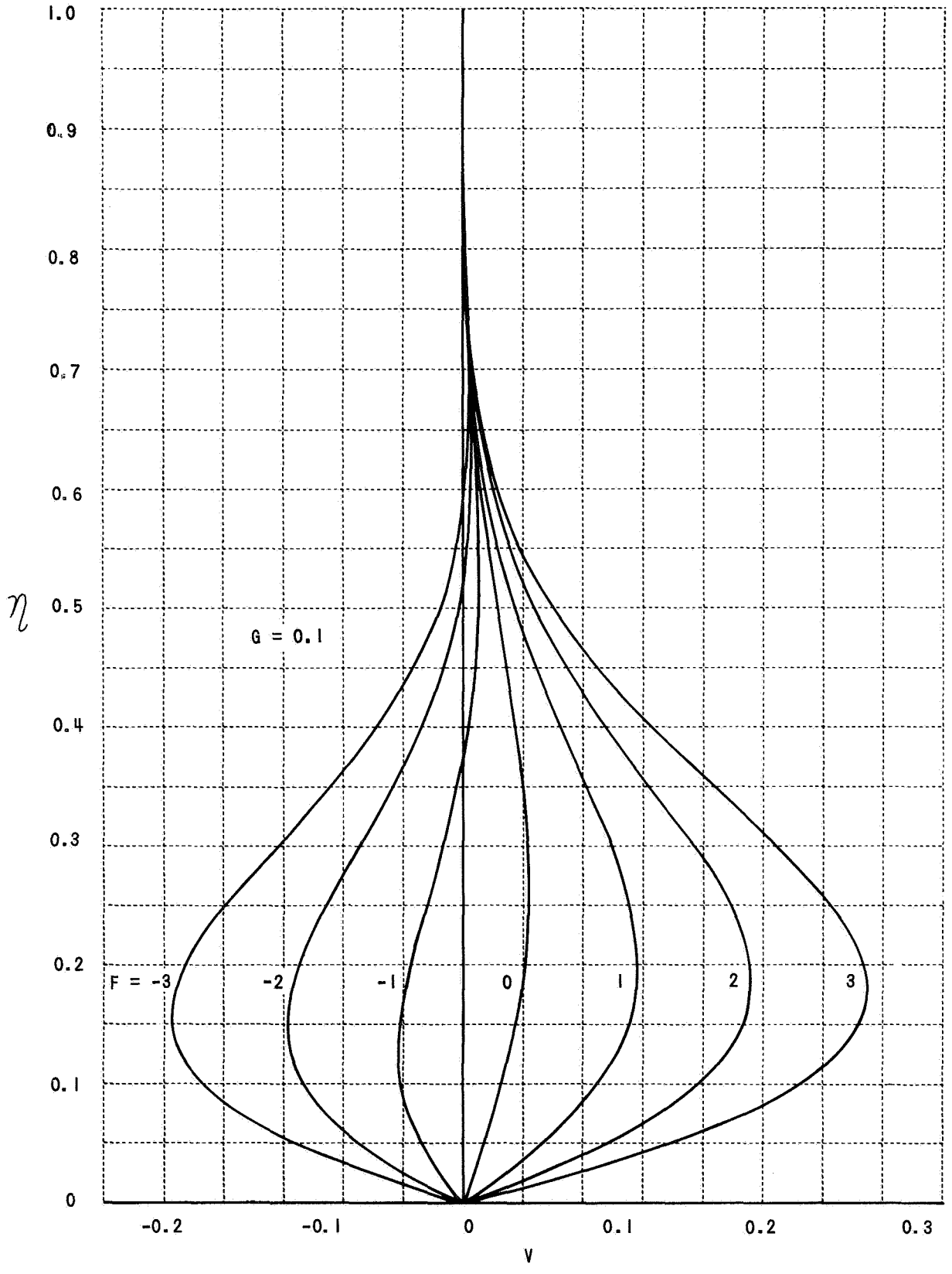

Figure 9 DISTRIBUTIONS OF THE SECONDARY-FLOW VELOCITY PROFILES (G = 0.1)

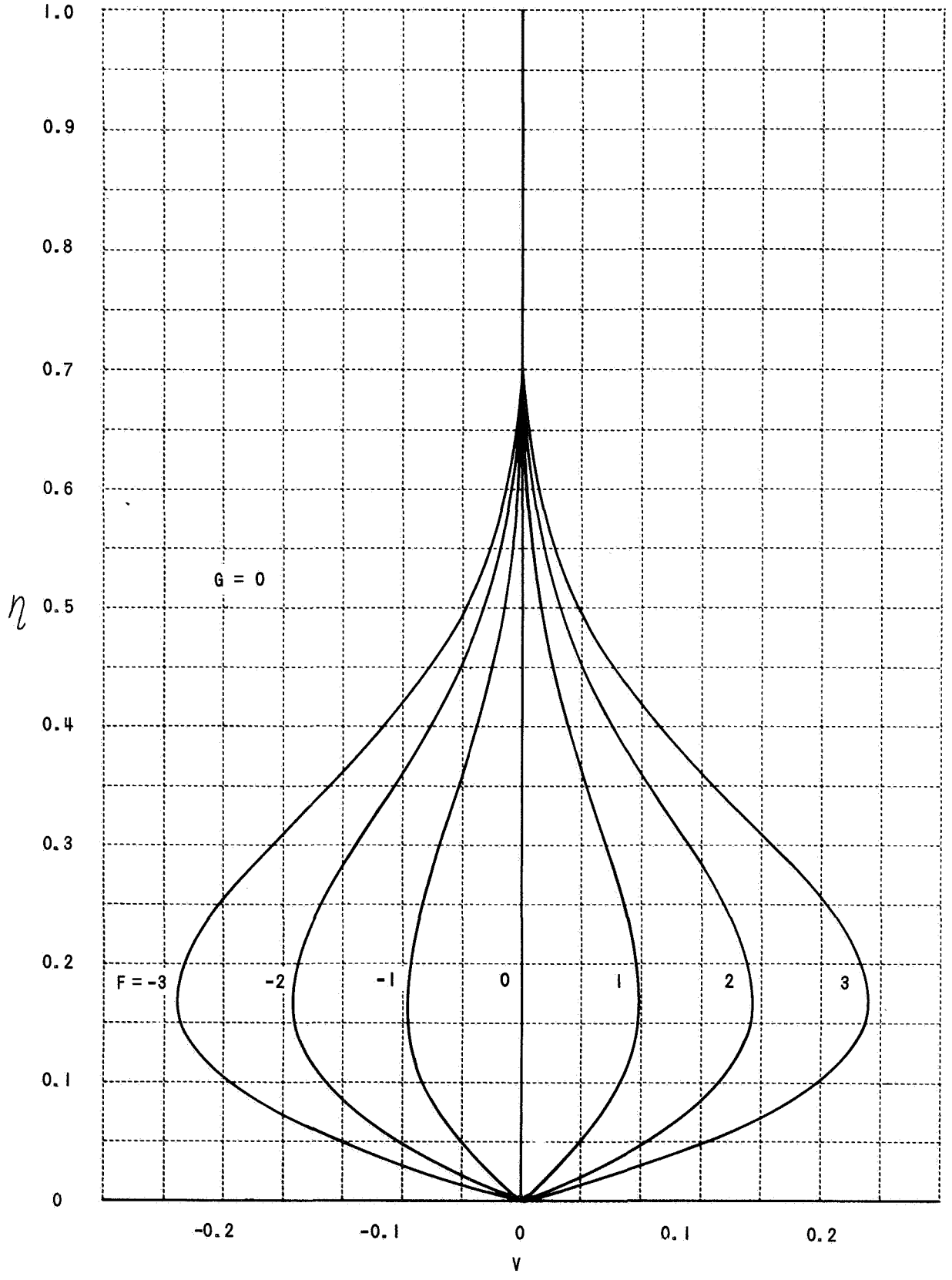

Figure 10 DISTRIBUTIONS OF THE SECONDARY-FLOW VELOCITY PROFILES (G = 0)

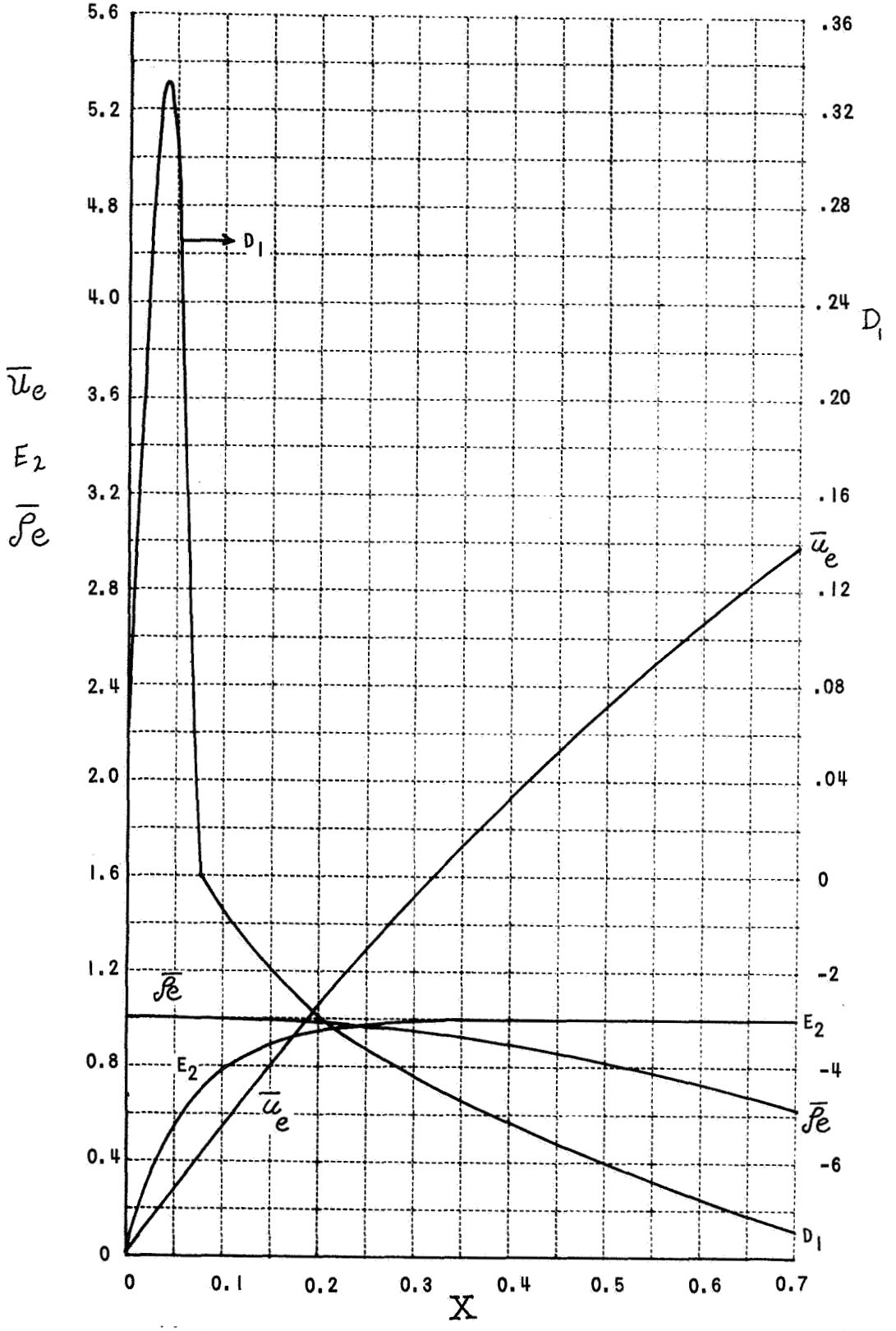

Figure 11 DISTRIBUTIONS OF FLOW PROPERTIES ALONG STREAMLINE

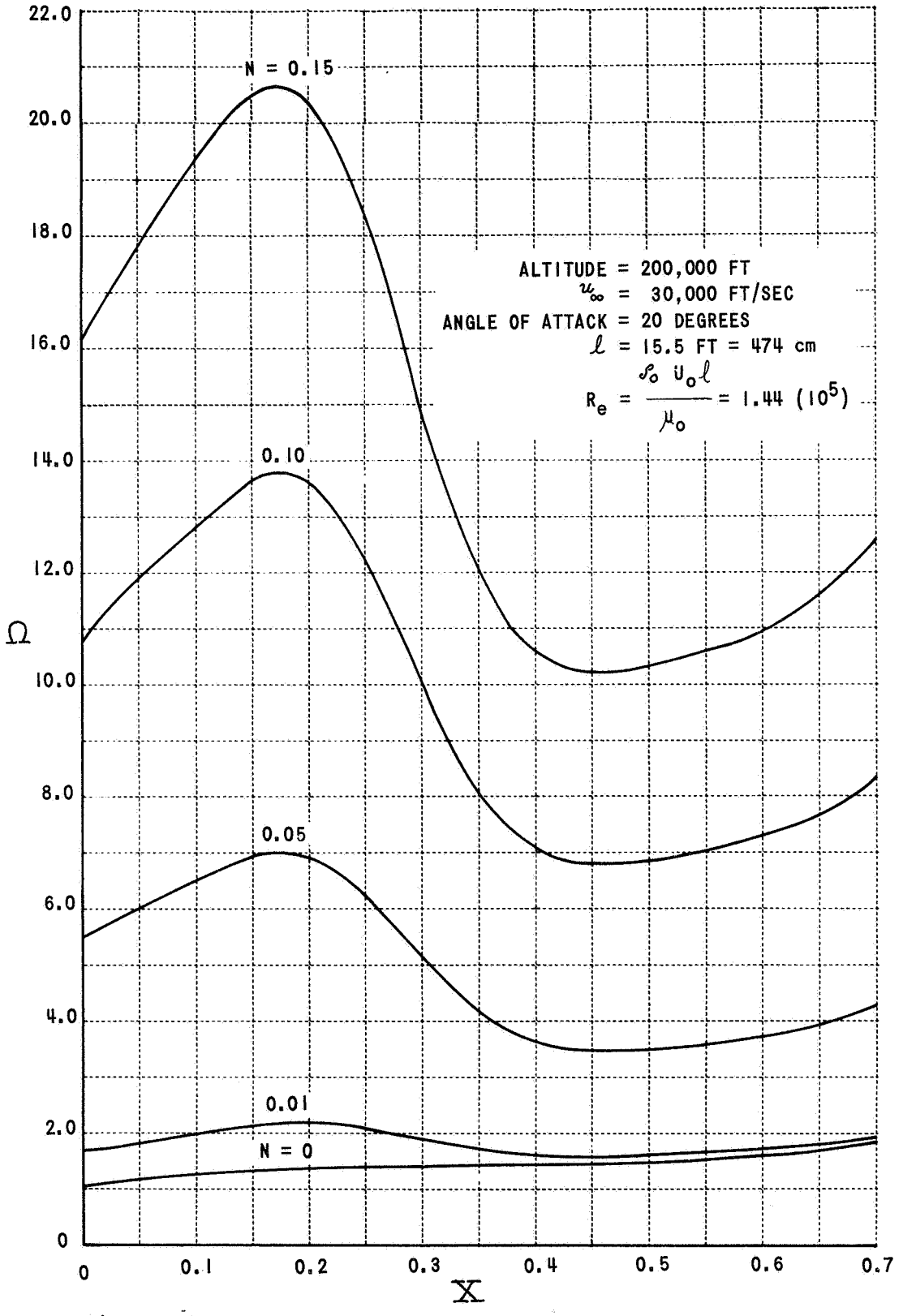

Figure 12 DISTRIBUTIONS OF "BOUNDARY-LAYER THICKNESS" ALONG STREAMLINE FOR VARIOUS MASS-INJECTION RATES

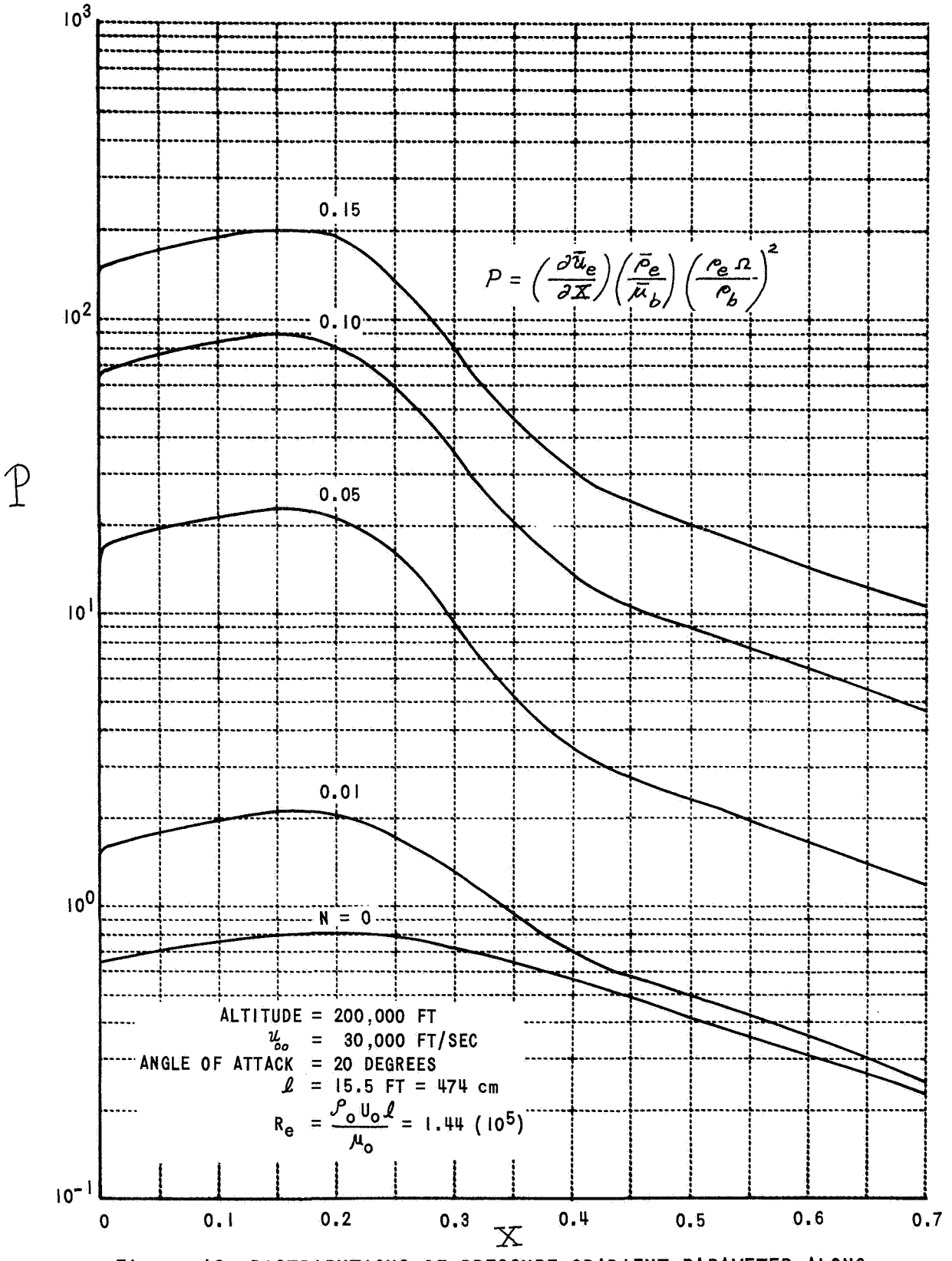

Figure 13 DISTRIBUTIONS OF PRESSURE-GRADIENT PARAMETER ALONG STREAMLINE FOR VARIOUS MASS-INJECTION RATES

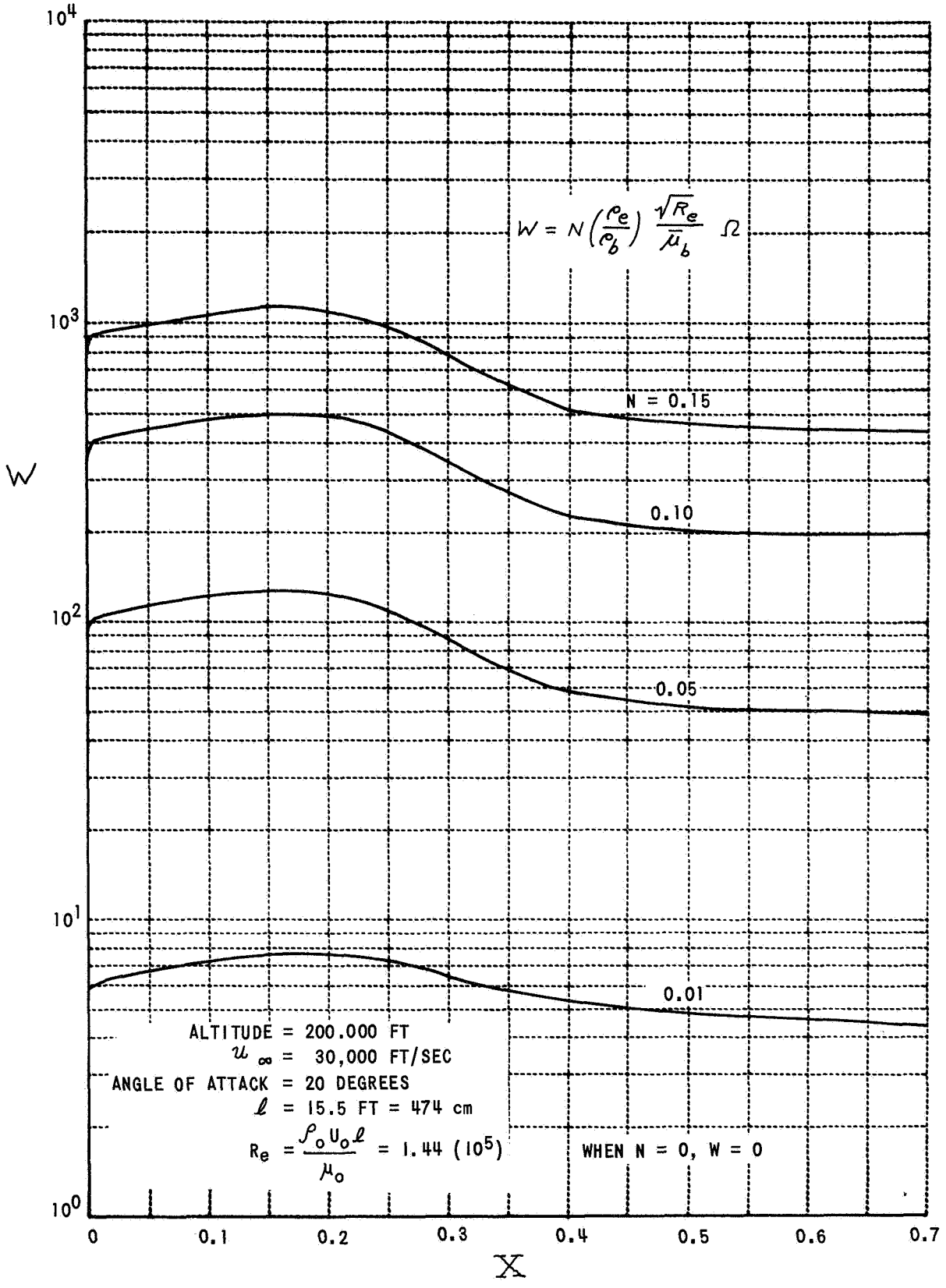

Figure 14 DISTRIBUTIONS OF MASS-INJECTION PARAMETER ALONG STREAMLINE

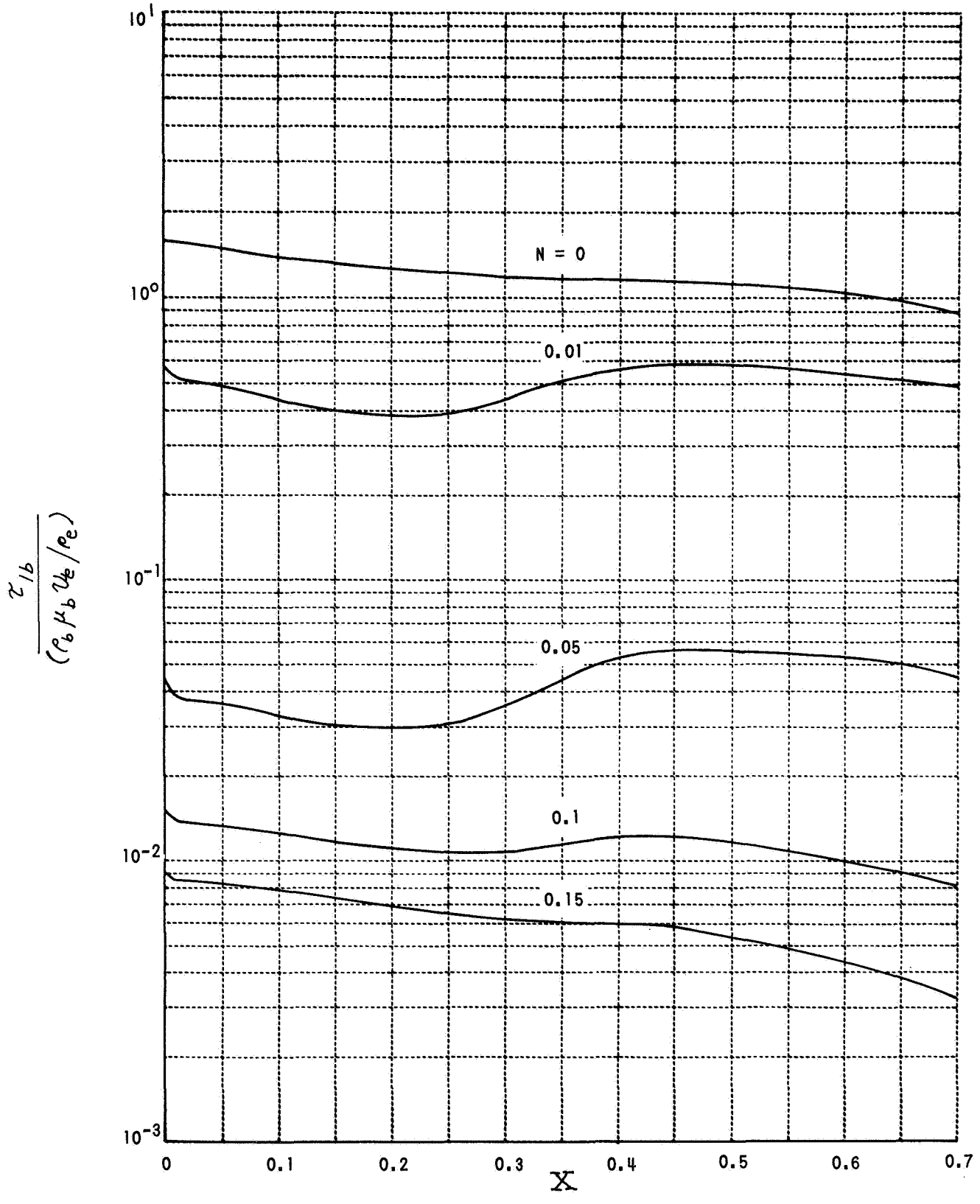

Figure 15 DISTRIBUTIONS OF STREAMWISE WALL-SHEAR ALONG STREAMLINE FOR VARIOUS MASS-INJECTION RATES

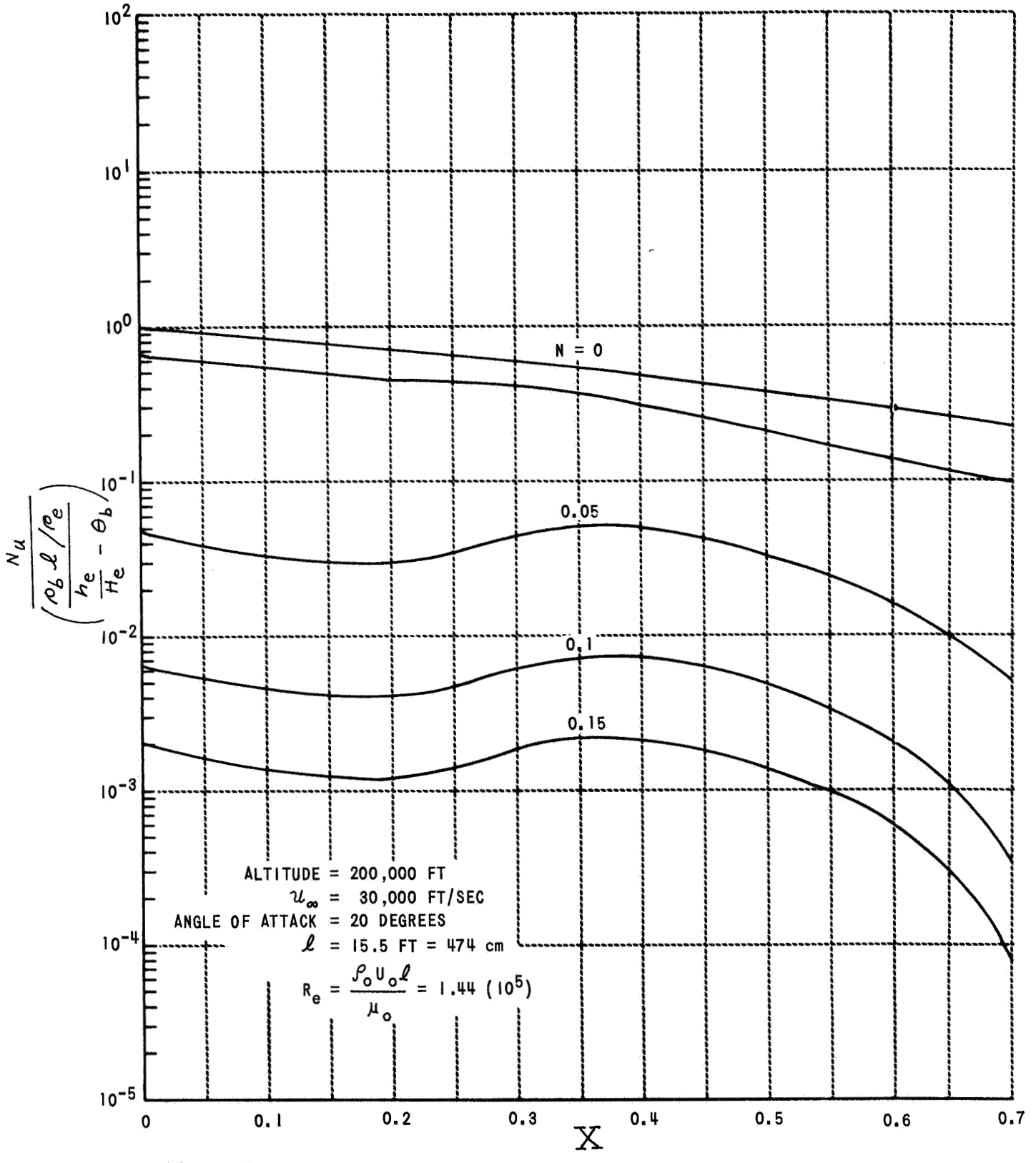

Figure 16 DISTRIBUTIONS OF HEAT TRANSFER PARAMETER ALONG STREAMLINE FOR VARIOUS MASS-INJECTION RATES

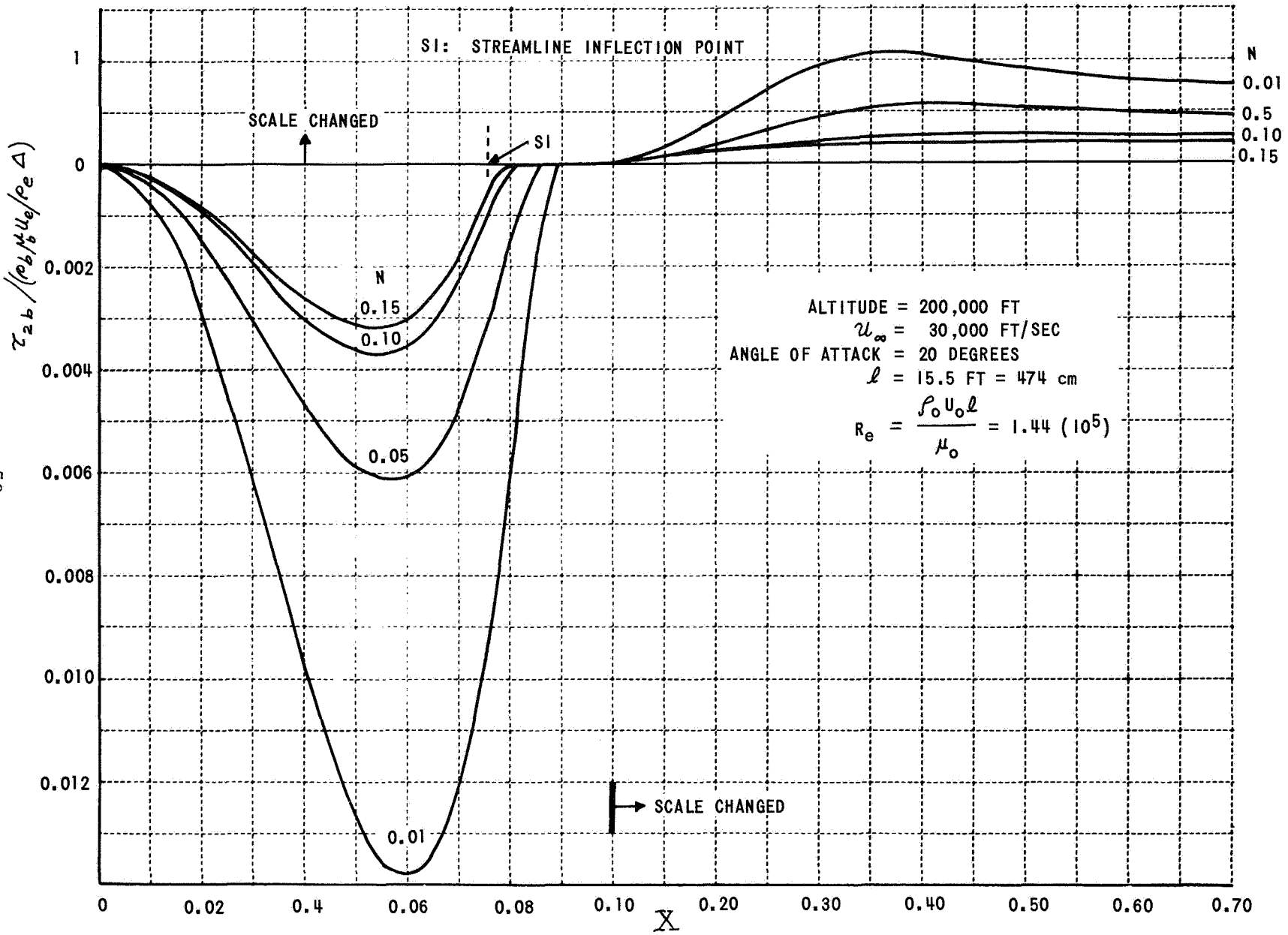

Figure 17A DISTRIBUTIONS OF TRANSVERSE WALL SHEAR ALONG STREAMLINE FOR VARIOUS MASS-INJECTION RATES

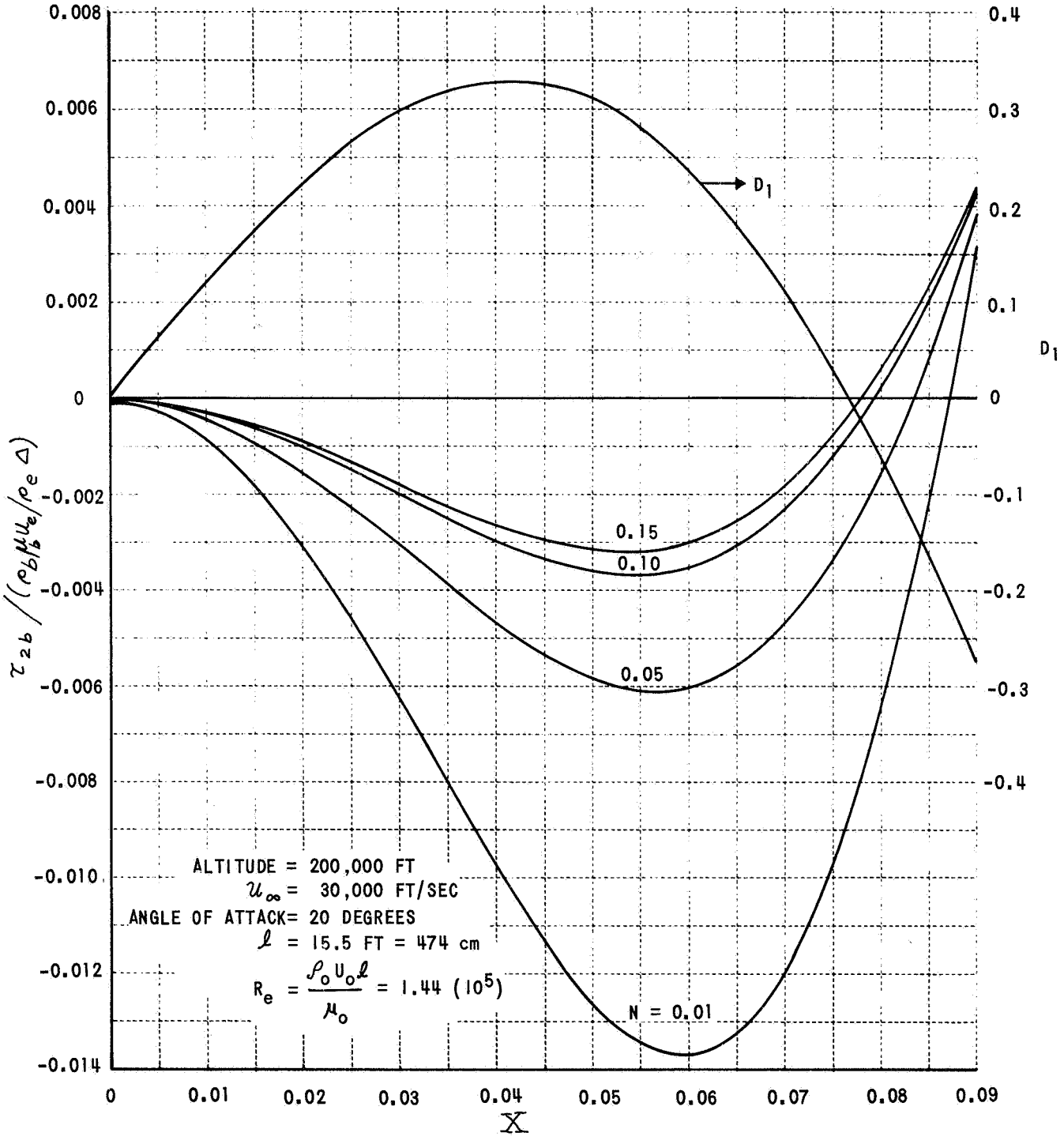

Figure 17B DISTRIBUTIONS OF TRANSVERSE WALL SHEAR ALONG STREAMLINE FOR VARIOUS MASS-INJECTION RATES